Fractals, Vol. 5, No. 4 (1997) 565–595


# Articles

# ANALYSIS, SYNTHESIS, AND ESTIMATION OF FRACTAL-RATE STOCHASTIC POINT PROCESSES

STEFAN THURNER, STEVEN B. LOWEN, MARKUS C. FEURSTEIN
and CONOR HENEGHAN
*Department of Electrical & Computer Engineering, Boston University, Boston, MA 02215*

HANS G. FEICHTINGER
*Institut für Mathematik, Universität Wien, A-1090 Vienna, Austria*

MALVIN C. TEICH*
*Departments of Electrical & Computer Engineering, Biomedical Engineering, and Physics, Boston University, Boston, MA 02215*

Received May 5, 1997; Accepted May 20, 1997

## Abstract

Fractal and fractal-rate stochastic point processes (FSPPs and FRSPPs) provide useful models for describing a broad range of diverse phenomena, including electron transport in amorphous semiconductors, computer-network traffic, and sequences of neuronal action potentials. A particularly useful statistic of these processes is the fractal exponent $\alpha$, which may be estimated for any FSPP or FRSPP by using a variety of statistical methods. Simulated FSPPs and FRSPPs consistently exhibit bias in this fractal exponent, however, rendering the study and analysis of these processes non-trivial. In this paper, we examine the synthesis and estimation of FRSPPs by carrying out a systematic series of simulations for several different types of FRSPP over a range of design values for $\alpha$. The discrepancy between the desired and achieved values of $\alpha$ is shown to arise from finite data size and from the character of the point-process generation mechanism. In the context of point-process simulation, reduction of this discrepancy requires generating data sets with either a large number of points, or with low jitter in the generation of the points. In the context of fractal data analysis, the results presented here suggest caution when interpreting fractal exponents estimated from experimental data sets.

*Corresponding author. Email address: teich@bu.edu; URL: http://ece.bu.edu/ECE/faculty/homepages/teich.html/

# 1. INTRODUCTION

Some random phenomena occur at discrete times c locations, with the individual events largely ident cal, such as a sequence of neural action potentials A stochastic point process[1] is a mathematical cor struction which represents these events as rando points in a space. Fractal stochastic point processe exhibit scaling in all of the statistics considered i this paper; fractal-rate stochastic point processe do so in some of them. In this work we consider th simulation and estimation of fractal and fractal-rat stochastic point processes on a line, which model variety of observed phenomena in the physical an biological sciences. This work provides an extensio and generalization of an earlier paper along thes lines.[2]

## 1.1 Mathematical Descriptions of Stochastic Point Processes

Figure 1 shows several representations that are useful in the analysis of point processes. Figure 1(a) demonstrates a sample function of a point process as a series of impulses occurring at specified times $t_n$. Since these impulses have vanishing width, they are most rigorously defined as the derivative of a well-defined counting process $N(t)$ [Fig. 1(b)], a monotonically increasing function of $t$, that augments by unity when an event occurs. Accordingly, the point process itself is properly written as $dN(t)$, since it is only strictly defined within the context of an integral.

The point process is completely described by the set of event times $\{t_n\}$, or equivalently by the set of interevent intervals. However, the sequence of counts depicted in Fig. 1(c) also contains much information about the process. Here the time axis is divided into equally spaced contiguous counting windows of duration $T$ sec to produce a sequence of counts $\{Z_k\}$, where $Z_k = N[(k+1)T] - N[kT]$ denotes the number of events in the $k$th window. As illustrated in Fig. 1(d), this sequence forms a discrete-time random process of nonnegative integers. In general, information is lost in forming the sequence of counts, although for a regular point process the amount lost can be made arbitrarily small by reducing the size of the counting window $T$. An attractive feature of this representation is that it preserves the correspondence between the discrete time axis of the counting process $\{Z_k\}$ and the absolute "real" time axis of the underlying point process.

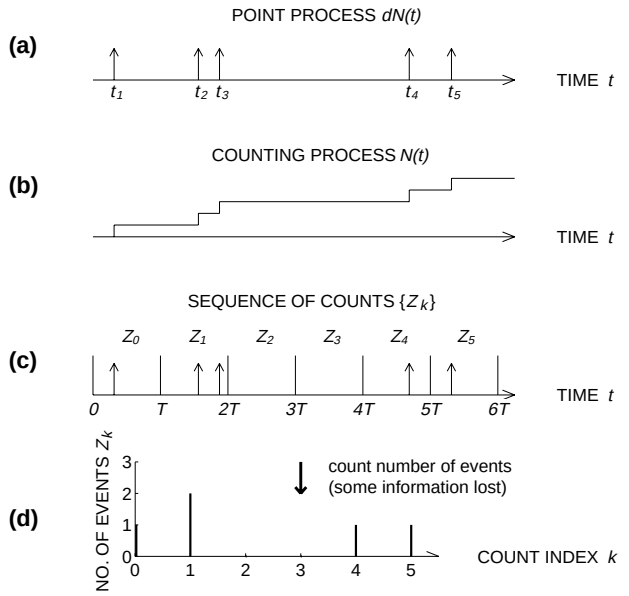


**Fig. 1** Representations of a point process. **(a)** The events are represented by a sequence of idealized impulses, occurring at times $t_n$, and forming a stochastic point process $dN(t)$. For convenience of analysis, several alternative representations of the point process are used. **(b)** The counting process $N(t)$. At every event occurrence the value of $N(t)$ augments by unity. **(c)** The sequence of counts $\{Z_k\}$, a discrete-time non-negative integer-valued stochastic process, is formed from the point process by recording the number of events in successive counting windows of length $T$. **(d)** The sequence of counts $\{Z_k\}$ can be conveniently described in terms of a count index $k$. Information is lost because the precise times of event occurrences within each counting window are eliminated in this representation. Correlations in the discrete-time sequence $\{Z_k\}$ can be readily interpreted in terms of real time.

Within the process of counts $\{Z_k\}$, the elements $Z_k$ and $Z_{k+n}$ refer to the number of counts in windows separated by precisely $T(n-1)$ sec, so that correlation in the process $\{Z_k\}$ is readily associated with correlation in the underlying point process $dN(t)$.

## 1.2 Scaling and Power-Law Behavior in Fractal Stochastic Processes

The complete characterization of a stochastic process involves a description of all possible joint probabilities of the various events occurring in the process. Different statistics provide complementary views of the process; no single statistic can in general describe a stochastic process completely. Fractal stochastic processes exhibit scaling in their statistics. Such scaling leads naturally to power-law

behavior, as demonstrated in the following. Consider a statistic $f$ which depends continuously on the scale $x$ over which measurements are taken. Suppose changing the scale by any factor $a$ effectively scales the statistic by some other factor $g(a)$, related to the factor but independent of the original scale:

$$f(ax) = g(a)f(x)\,. \tag{1}$$

The only nontrivial solution of this scaling equation for real functions and arguments, that is independent of $a$ and $x$ is

$$f(x) = bg(x) \qquad \text{with} \qquad g(x) = x^c \tag{2}$$

for some constants $b$ and $c$.[2,3] Thus statistics with power-law forms are closely related with the concept of a fractal. The particular case of fixed $a$ admits a more general solution:[4]

$$g(x;a) = x^c\,\cos[2\pi\ln(x)/\ln(a)]\,. \tag{3}$$

### 1.3 Fractal Stochastic Point Processes (FSPPs)

Consider, for example, a commonly encountered first-order statistic for a stochastic point process, the interevent interval histogram (IIH). This estimates the interevent-interval probability density function (IIPDF) $p(t)$ by computing the relative frequency of occurrence of interevent intervals as a function of interval size. This measure highlights the behavior of the times between adjacent events, but reveals none of the information contained in the relationships among these times, such as that correlation between adjacent time intervals. For a fractal stochastic point process (FSPP) the IIPDF follows the form of Eq. (2), so that $p(t) \sim t^c$ over a certain range of $t$, where $c < -1$.

A number of statistics may be used to describe an FSPP, and each statistic which scales will in general have a different scaling exponent $c$. Each of these exponents can be simply related to a more general parameter $\alpha$, the fractal exponent, where the exact relation between these two exponents will depend upon the statistic in question. For example, the exponent $c$ of the IIPDF defined above is related to the fractal exponent $\alpha$ by $c = -(1+\alpha)$.

Sample functions of the fractal renewal point process (FRP; see Sec. 4.1) are true fractals; the expected value of their generalized dimensions (see Sec. 3.2) assumes a nonintegral value between the topological dimension (zero) and the Euclidean dimension (unity).[5]

### 1.4 Fractal-Rate Stochastic Point Processes (FRSPPs)

However, the sequence of unitary events observed in many biological and physical systems do not exhibit power-law-distributed IIHs but nevertheless exhibit scaling in other statistics. These processes therefore have integral generalized dimensions (see Sec. 3.2) and are consequently not true fractals. They are nevertheless endowed with rate functions that are indeed either fractals or their increments: fractal Gaussian noise, fractal Brownian motion, or closely related processes. Therefore, such point processes are more properly termed fractal-*rate* stochastic point processes (FRSPPs).

### 1.5 Relation of Fractal Exponent to Hurst Exponent

The fractal exponent $\alpha$ defined above is related to the more commonly encountered Hurst exponent $H$.[6] The relationship is ambiguous, however, since some authors[5,7–10] use the formula $\alpha = 2H + 1$ for all values of $\alpha$, while others[11] use $\alpha = 2H - 1$ for $\alpha < 1$ to restrict $H$ to the range $(0, 1)$. In this paper, we avoid this confusion by considering $\alpha$ directly instead of $H$.

## 2. APPLICATIONS OF FRACTAL AND FRACTAL-RATE STOCHASTIC POINT PROCESSES

Many phenomena are readily represented by FSPPs and FRSPPs. We provide several examples drawn from the physical[12–14] and biological[15–17] sciences.

### 2.1 Trapping Times in Amorphous Semiconductors

A multiple trapping model has been used to show how traps that are exponentially distributed over a large range of energies lead to a power-law decay of current in an amorphous semiconductor.[18–22] If a pulse of light strikes such a semiconductor, the many carriers excited out of their traps will be

available to carry current until they are recaptured, which happens relatively quickly. At some point each carrier will be released from its trap by thermal excitation and become mobile for a time, and then be recaptured by another trap. For exponentially distributed energy states with identical capture cross sections, the electrons tend to be trapped in shallow states at first, but the probability of being caught in a deep trap increases as time progresses. This leads to a current that decreases as a power-law function of time.

The multiple trapping model may be usefully recast in terms of a standard fractal renewal process (see Sec. 4.1).[23,24] Consider an amorphous semiconductor with localized states (traps) with energies which are exponentially distributed with parameter $E_0$ between a minimum energy $E_L$ of the order of $\kappa\mathcal{T}$, where $\kappa$ is Boltzmann's constant and $\mathcal{T}$ is the temperature in degrees Kelvin; and a maximum energy $E_H$ determined by the bandgap of the material. For a particular trap with energy $\mathcal{E}$, the corresponding mean waiting time to release is

$$\tau = \tau_0 \exp(\mathcal{E}/\kappa\mathcal{T}) , \tag{4}$$

where $\tau_0$ is the average vibrational period of the atoms in the semiconductor. If we define characteristic time cutoffs $A \equiv \tau_0 \exp(E_L/\kappa\mathcal{T})$ and $B \equiv \tau_0 \exp(E_H/\kappa\mathcal{T})$, and the power-law exponent $c \equiv \kappa\mathcal{T}/E_0$, then the mean waiting time $\tau$ has a density which decays as a power law with this exponent between those two cutoffs. Each trap holds carriers for times that are exponentially distributed given the conditional parameter $\tau$, and averaging this exponential density over all possible values of $\tau$ yields the unconditional trapping time density, which is itself approximately power law:

$$p(t) \approx c\Gamma(c+1)A^c t^{-(c+1)}, \tag{5}$$

for $A \ll t \ll B$. Thus each carrier will be trapped for a period that is essentially power-law distributed.

Upon escaping from a trap, the carrier can conduct current for a short time until it is again captured by another trap. Thus each carrier executes a series of current-carrying jumps well described by a standard FRP. Assuming that each carrier acts independently of the others, the action of the carriers as a whole can be modeled as the superposition of a collection of such component processes, which converges to the fractal-Gaussian-noise driven Poisson process (FGNDP; see Secs. 4.2.1 and 4.4) in the limit of a large number of carriers. Again, both experimental[25] and theoretical[22,26] results point to a power-law or fractal decay in the power spectral density, while several other statistics also show scaling behavior.

## 2.2 Noise and Traffic in Communications Systems

Burst noise occurs in many communications systems and is characterized by relatively brief noise events which cluster together, separated by relatively longer periods of quiet. Berger and Mandelbrot[27,28] showed long ago that burst errors in communication systems are well modeled by a version of a fractal renewal process (see Sec. 4.1), and in particular that the interevent times were essentially independent of each other for time scales determined by the resolution and the duration of the observation.

Moreover, the rate of traffic flow itself displays fractal fluctuations on a variety of high-speed packet-switching networks conducting different types of traffic.[29–33] This has been demonstrated for time scales greater than about one sec, in both the power spectral density and the Fano factor (see Secs. 3.4 and 3.5). Over these time scales, the fractal-shot-noise driven Poisson process (FSNDP; see Secs. 4.2.5 and 4.4) has been successfully employed to model the traffic.[34]

## 2.3 Current Flow in Biological Ion Channels

Ion channels reside in biological cell membranes, permitting ions to diffuse in or out.[35] These channels are usually specific to a particular ion, or group of related ions, and block the passage of other kinds of ions. Further, most channels have gates, and thus the channels may be either open or closed. In many instances, intermediate conduction states are not observed. Some ion channels may be modeled by a two-state Markov process,[36] with one state representing the open channel, and the other representing the closed channel. This model generates exponentially distributed dwell times in both states, which are, in fact, sometimes observed. However, many ion channels exhibit independent

power-law distributed closed times between open times of negligible duration,[37–40] and are well described by a fractal renewal point process (see Sec. 4.1).[41,42]

## 2.4 Vesicular Exocytosis at the Synaptic Cleft

Communication in the nervous system is usually mediated by the exocytosis of multiple vesicular packets (quanta) of neurotransmitter molecules at the synapse between two cells, triggered by an action potential (information-bearing signal) at the presynaptic cell.[43] Even in the absence of an action potential, however, many neurons spontaneously release individual packets of neurotransmitter.[44] On arrival at the postsynaptic membrane, each neurotransmitter packet induces a miniature endplate current (MEPC); superpositions of MEPC-like events comprise the postsynaptic endplate currents elicited by nerve impulses arriving at the presynaptic cell.[45] Analysis of the sequence of MEPC and MEPC-like events in a variety of preparations reveals the presence of memory over a range of times and frequencies.[46] The fractal-lognormal-noise driven Poisson process model (FLNDP; see Secs. 4.2.2 and 4.4) provides an excellent model for this process, for a variety of statistical measures.[46,47]

## 2.5 Action Potentials in Isolated Neuronal Preparations

Many biological neurons carry information in the form of sequences of action potentials, which are localized regions of depolarization traveling down the length of an axon. Action potentials or neural spikes are brief and largely identical events and are well represented by a point process. The firing patterns of an isolated neuron and an isolated axons have been shown to have fractal characteristics. Musha and colleagues generated a synthetic spike train consisting of electrical impulses separated by independent intervals drawn from the same Gaussian distribution.[48] This nonfractal stimulus as applied to one end of an excised squid giant axon; the membrane voltage at the far end was considered to be the response spike train. The resulting power spectral density followed a $1/f$-type decay. Spontaneous firing from an excised giant snail neuron yielded similar results,[49] although for this preparation the data was selected to reduce fluctuations, and analyzed by interevent number rather than in real time.

## 2.6 Auditory-Nerve-Fiber Action Potentials

More recently, fractal behavior has been observed in the sequence of action potentials recorded from several *in vivo* vertebrate preparations. Real-time recordings were made under both spontaneous and driven firing conditions. Over short time scales, nonfractal stochastic point processes prove adequate for representing such nerve spikes, but over long time scales (typically greater than one sec) the fractal nature becomes evident.[50] Estimators of the rate of the process converge more slowly than for nonfractal processes, displaying fluctuations which decrease as a power-law function of the time used to estimate the rate.[51] With the inclusion of the refractory effects of nerve fibers, FRSPP models have been shown to properly characterize the statistical properties of certain potentials in peripheral primary auditory fibers in several species, over all time scales and for a broad variety of statistical measures;[40,51–62] only four parameters are required. This process possibly arises from superpositions of fractal ion-channel transitions[41,42] or by fractal vesicular exocytosis in inner-ear sensory cells, as described briefly in Secs. 2.3 and 2.4, respectively.

## 2.7 Optic-Nerve-Fiber Action Potentials

Many neurons in the mammalian visual system transmit information by means of action potentials as well, and FRSPPs also provide suitable models for describing the behavior of these neurons.[63] The gamma renewal process, which is nonfractal, has proven to be a useful model for some of these processes over short time scales.[64] However, nerve spike trains recorded from both cat retinal-ganglion-cell and lateral-geniculate-nucleus neurons, like those recorded from primary auditory neurons, exhibit fractal behavior over time scales greater than about 1 sec, thus necessitating the use of an FRSPP description.[63] Long-duration temporal correlation has also been observed in spike trains from cat

striate-cortex neurons[65] and from an insect visual interneuron.[66]

### 2.8 Central-Nervous-System Action Potentials

Action-potential data collected from rabbit somatosensory cortical neurons and cat respiratory control neurons show experimental IIH plots which decay as power laws.[67] In addition, for the data lengths considered, serial correlation coefficients among interevent intervals from these data sets do not differ from zero in a statistically significant way. (However, differences may well emerge for longer data sets, as has been seen, for example, in auditory-nerve-fiber recordings.[50]) These two interevent-interval characteristics — independence and a power-law distribution — define the fractal renewal point process (see Sec. 4.1), which is an FSPP.

On the other hand, action potentials in the cat mesencephalic reticular formation (MRF) exhibit activity that can be modeled by an FRSPP. During REM phases of sleep, these neurons exhibit $1/f$-type spectra,[68–70] as do certain hippocampal and thalamic neurons.[71] The cluster Poisson point process (see Sec. 4.5) has been used successfully to model MRF neural activity.[70] Furthermore, there is some evidence that these neurons have IIHs whose tails decay in power-law fashion,[72] so that a type of FSPP may prove suitable for describing these spike trains.

### 2.9 Human Heartbeat Times

The sequence of human heartbeats exhibits considerable variability over time, both in the short-term and in the long-term patterns of the times between beats.[73,74] A point process of the heartbeats is formed by focusing on the times between maximum contractions (R-R intervals). A particular FRSPP with an integrate-and-fire substrate has been constructed and shown to successfully describe these events.[75,76] As with auditory and visual-system spike trains, over short time scales nonfractal point processes provide suitable models for the pattern of times between contractions; for times longer than roughly 10 sec, only fractal models suffice. Interestingly, parameters of the FRSPP used to model the data indicate promise for the diagnosis of various disease states of the heart.[76]

## 3. ANALYSIS OF FRACTAL-RATE STOCHASTIC POINT PROCESSES

As the examples described above illustrate, many phenomena are amenable to modeling by FRSPPs. The value of the fractal exponent $\alpha$ can often provide important information regarding the nature of an underlying process, and can also serve as a useful classification tool in some cases, as with human heartbeat data as mentioned in Sec. 2.9. Accordingly, it is desirable to estimate $\alpha$ reliably, although this task is often confounded by a variety of issues.[2,77,78]

Here we briefly review some of the techniques used for estimating $\alpha$. By way of illustration, we apply these methods to a train of action potentials recorded from a lateral-geniculate-nucleus (LGN) relay neuron in the cat visual system. There are 24285 events in this particular spike train, with an average interevent interval of 0.133 sec, comprising a total duration of 3225 sec.[63]

### 3.1 Interval Probability Density Function

The interevent-interval histogram (IIH), an estimate of the interval probability function, and the generalized dimension (GD),[79–81] are useful measures for fractal stochastic point processes, and in particular for the fractal renewal process (see Sec. 4.1). The IIH is simply the relative frequency of interevent-interval occurrence in the data set, ignoring all correlations among the intervals.

Since realizations of FSPPs form true fractals, all measures considered in this paper, including the IIH, exhibit scaling for these processes. Thus the IIH proves useful in elucidating the fractal nature of FSPPs. For FRSPPs, on the other hand, the fractal structure is not manifested in first-order interevent-time statistics, so that the IIH does not scale over a significant range of interevent times. Rather, the fractal character of these processes lie in the dependencies among the interevent intervals, which are captured by the measures considered in Secs. 3.3–3.6.

### 3.2 Generalized Dimension

The generalized dimension is of interest for fractal stochastic point processes. If a data segment of

length $L$ is divided into intervals of length $T$, with $Z_k$ representing the number of points in the $k$th interval [see Fig. 1(c)], then the generalized dimension $D_q$ of a point process is defined as

$$D_q \equiv \frac{1}{q-1} \lim_{T \to 0} \frac{\log\left(\sum Z_k^q\right)}{\log(T)}, \qquad (6)$$

where the sum extends over all non-empty intervals. Particular cases are the capacity or box-counting dimension $D_0$, the information dimension $\lim_{q \to 1} D_q$, and the correlation dimension $D_2$. The sum is a form of time averaging; for a stochastic point process, it is convenient to replace the sum by the product of $L/T$ and the expected value of $Z^q$. For a fractal-rate point process, however, analytical values of the $D_q$ will not in general equal analytical values of the dimensions obtained from the periodogram or Allan Factor, and in fact the $D_q$ will often assume integer values (see Sec. 1.4).

### 3.3 Coincidence Rate

The Coincidence Rate (CR) measures the correlations between pairs of events with a specified time delay between them, regardless of intervening events, and is related to the autocorrelation function used with continuous processes. The CR is defined as

$$G(\tau) \equiv \lim_{\Delta \to 0} \frac{\Pr\left\{\mathcal{E}[0, \Delta] \text{ and } \mathcal{E}[\tau, \tau + \Delta]\right\}}{\Delta^2}, \qquad (7)$$

where $\mathcal{E}[s, t]$ denotes the occurrence of at least one event of the point process in the interval $[s, t)$ and $\tau$ is the delay time. For an ideal fractal or fractal-rate stochastic point process with a fractal exponent $\alpha$ in the range $0 < \alpha < 1$, the coincidence rate assumes the form[2]

$$G(\tau) = \lambda \delta(\tau) + \lambda^2 \left[1 + (\mid \tau \mid / \tau_0)^{\alpha - 1}\right], \qquad (8)$$

where $\lambda$ is the mean rate of the process, $\delta(\tau)$ denotes the Dirac delta function, and $\tau_0$ is a constant representing the fractal onset time.

A stationary, regular point process with a CR following this form for *all* delay times $\tau$ exhibits infinite mean. Further, statistics of fractal data sets collected from experiments exhibit scaling only over a finite range of times and frequencies, as determined by the resolution of the experimental apparatus and the duration of the experiment. Nevertheless, in much of the following we employ Eq. (8) without cutoffs since we find that the cutoffs do not significantly affect the mathematical results in many cases. We employ similar ideal forms for other second-order measures defined later in this paper for the same reasons.

The coincidence rate can be directly estimated from its definition. However, in practice the CR is a noisy measure, since its definition essentially involves a double derivative. Furthermore, for FSPPs and FRSPPs typical of physical and biological systems, the CR exceeds its asymptotic value $\lambda^2$ by only a small fraction at any large but practical value of $\tau$, so that determining the fractal exponent with this small excess presents serious difficulties. Therefore we do not specifically apply this measure to the LGN data, although the formal definition of coincidence rate plays a useful role in developing other, more reliable measures.

### 3.4 Power Spectral Density

The power spectral density (PSD) is a familiar and well-established measure for continuous-time processes. For point processes the PSD and the CR introduced above form a Fourier transform pair, much like the PSD and the autocorrelation function do for continuous-time processes. The PSD provides a measure of how the power in a process is concentrated in various frequency bands. For an ideal fractal point process, the PSD assumes the form

$$S(\omega) = \lambda^2 \delta(\omega / 2\pi) + \lambda \left[1 + (\omega / \omega_0)^{-\alpha}\right], \qquad (9)$$

for relevant time and frequency ranges, where $\lambda$ is the mean rate of events and $\omega_0$ is a cutoff radian frequency.

The PSD of a point process can be estimated using the periodogram (PG) $S_Z(\omega)$ of the sequence of counts, rather than from the point process itself.[82] This method introduces a bias at higher frequencies, since the fine time resolution information is lost as a result of the minimum count-window size. Nevertheless, since estimating the fractal exponent principally involves lower frequencies where this bias is negligible, and employing the sequence of counts permits the use of vastly more efficient fast Fourier transform methods, we prefer this technique. Alternate definitions of the PSD for point processes (and thus for the PG used to estimate them) exist; for example, a different PSD may be obtained from the real-valued discrete-time sequence of the interevent intervals. However, features in this PSD cannot be interpreted in terms of temporal frequency.[76]

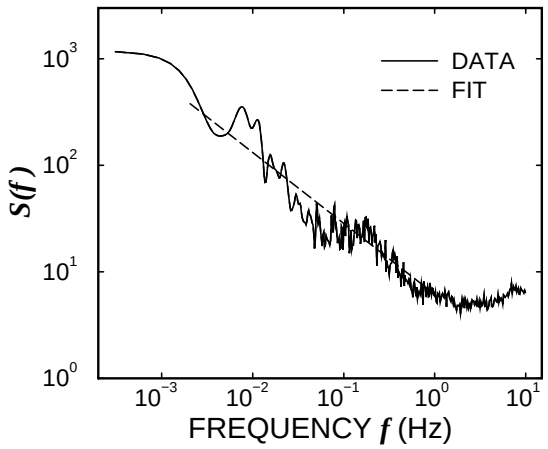


**Fig. 2** Doubly logarithmic plot of the count-based periodogram vs. frequency for the point process representing a spontaneous nerve spike train recorded at the output of a visual-system relay neuron in the lateral geniculate nucleus (LGN) of the cat (solid curve, cell No. MDS-LGN, X-ON type[63]). No external stimulus was present. The data segment analyzed here consists of 24285 events with an average interevent time of 0.133 sec, comprising a total duration of 3225 sec. Over long time scales (low frequencies), the curve can be fit by a straight line (dotted) of slope -0.67, representing fractal behavior. This least-squares straight-line fit to the data was calculated over the region from 0.002 Hz to 1 Hz.

Figure 2 displays the PG for the visual system LGN data calculated using the count-based approach. Throughout the text of this paper we employ radian frequency $\omega$ (radians per unit time) to simplify the analysis, while figures are plotted in common frequency $f = \omega/2\pi$ (cycles per unit time) in accordance with common usage. For low frequencies, the PG decays as $1/\omega^{\alpha}$, as expected for a fractal point process. Fitting a straight line (shown as dotted) to the doubly logarithmic plot of the PG, over the range from 0.002 Hz to 1 Hz, provides an estimate $\widehat{\alpha} \approx 0.67$.

### 3.5 Fano Factor

Another measure of correlation over different time scales is provided by the Fano factor (FF), which is the variance of the number of events in a specified counting time $T$ divided by the mean number of events in that counting time. This measure is sometimes called the index of dispersion of counts.[1] In terms of the sequence of counts illustrated in Fig. 1(c), the Fano factor is simply the variance of $\{Z_k\}$ divided by the mean of $\{Z_k\}$, i.e.,

$$F(T) \equiv \frac{\mathrm{E}[Z_k^2] - \mathrm{E}^2[Z_k]}{\mathrm{E}[Z_k]}\,, \tag{10}$$

where $E[\cdot]$ represents the expectation operation. The FF may be obtained from the coincidence rate by an integral transform

$$F(T) = 1 + \frac{2}{\lambda T}\int_{0+}^{T}(T-\tau)\left[G(\tau) - \lambda^2\right]\,d\tau\,, \tag{11}$$

where $\lambda$ is the average rate of events of the point process, and the lower limit of the integral approaches zero from the positive side.[1]

The FF varies as a function of counting time $T$. The exception is the homogeneous Poisson point process (HPP), which is important as a benchmark in point-process theory just as the Gaussian is in the theory of continuous stochastic processes. For an HPP, the variance-to-mean ratio is always unity for any counting time $T$. Any deviation from unity in the value of $F(T)$ therefore indicates that the point process in question is not Poisson in nature. An excess above unity reveals that a sequence is less ordered than an HPP, while values below unity signify sequences which are more ordered. For an ideal FSPP or FRSPP with $0 < \alpha < 1$, the FF assumes the form

$$F(T) = 1 + (T/T_0)^{\alpha}\,, \tag{12}$$

where $T_0$ is a fractal onset time that differs from $\tau_0$ in Eq. (8) [see Eq. (17)]. Therefore a straight-line fit to an estimate of $F(T)$ vs. $T$ on a doubly logarithmic plot can also be used to estimate the fractal exponent. However, the estimated slope of the FF saturates at unity, so that this measure finds its principal applicability for processes with $\alpha < 1$.[2,60,63,83]

Figure 3 shows the estimated FF curve for the same data set as shown in Fig. 2. For counting times $T$ greater than approximately 0.3 sec, this curve behaves essentially as $\sim T^{\alpha}$. The estimated value is $\widehat{\alpha} = 0.66$ (dotted line), closely agreeing with the value obtained from the PG. Fair agreement between these two measures exists in other sensory spike-train and heartbeat sequence data sets[55,63,76] and in simulated FRSPPs.[2]

### 3.6 Allan Factor

The Allan variance, as opposed to the ordinary variance, is defined in terms of the variability of *successive* counts.[84,85] In analogy with the Fano factor

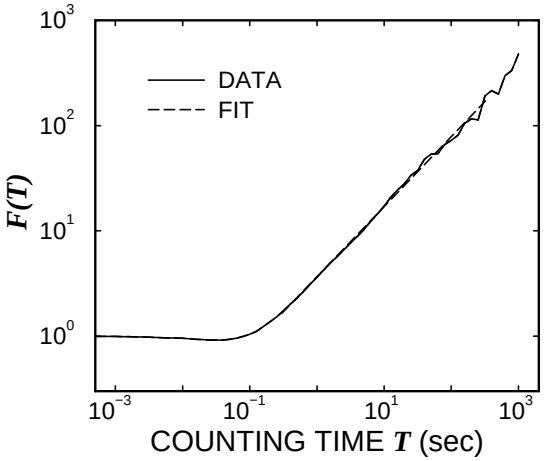


**Fig. 3** Doubly logarithmic plot of the Fano factor estimate vs. counting time, for the same spike train as used in Fig. 2 (solid curve). Over long time scales, the curve can be fit by a straight line (dotted) of slope 0.66, representing fractal behavior with a similar exponent to that obtained from the PG. This straight-line best fit to the data (on doubly logarithmic coordinates) was calculated over the region from 0.3 sec to 322 sec.

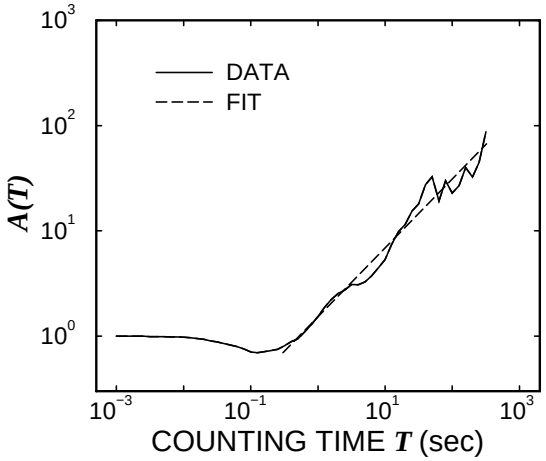


**Fig. 4** Doubly logarithmic plot of the Allan factor estimate vs. counting time for the same spike train as used in Figs. 2 and 3 (solid curve). Over long time scales, the curve can be fit by a straight line (dotted) of slope 0.65, representing fractal behavior with a similar exponent to that obtained from the PG and the FF. This straight-line best fit to the data (on doubly logarithmic coordinates) was calculated over the region from 0.3 sec to 322 sec.

(FF), we define the Allan factor (AF) for the sequence of counts shown in Fig. 1 as

$$A(T) \equiv \frac{\mathrm{E}\left[(Z_{k+1} - Z_k)^2\right]}{2\mathrm{E}[Z_k]} \,. \tag{13}$$

In terms of quantities defined earlier, we have

$$\begin{aligned} A(T) &= 2F(T) - F(2T) \\ &= 1 + \frac{4}{\lambda T} \int_{0+}^{T} (T - \tau) \left[G(\tau) - G(2\tau)\right] d\tau \,. \end{aligned} \tag{14}$$

As for the FF, the value of the Allan factor for the HPP is unity. For an ideal FRSPP with $0 < \alpha < 3$, the AF also assumes a power-law-varying form

$$A(T) = 1 + (T/T_1)^{\alpha} \,, \tag{15}$$

where $T_1$ is another fractal onset time, different from $\tau_0$ and $T_0$ [see Eq. (18)]; therefore a straight line fit of an estimate of $A(T)$ vs. $T$ on a doubly logarithmic plot yields yet another estimate of the fractal exponent.

Figure 4 shows the estimated Allan factor curve for the same data set as shown in Figs. 2 and 3. From visual inspection, this measure appears to be considerably "rougher" than the FF, which is typical of the data sets we have analyzed. Nevertheless it is clear that for counting times $T$ greater than approximately 0.3 sec, its behavior can also be approximated as $\sim T^{\alpha}$. To estimate the value of $\alpha$, a straight line fit to the doubly logarithmic plot of the estimate of $A(T)$ vs. counting time $T$ was provided. The value of $\widehat{\alpha} = 0.65$ obtained agrees well with the values calculated using the PG and FF. Excellent agreement between the AF and the PG exists in other sensory spike-train and heartbeat sequence data sets[60,63,76,86] and simulations.[63] Furthermore, the AF appears to yield superior estimates of $\alpha$ than the FF in all cases.[60,63,76,86] In particular, instead of saturating at a power-law exponent of unity, estimates of $\alpha$ obtained from the AF can range up to a value of three.[60] Thus we do not employ the FF in the remaining sections of this paper.

The Allan variance, $\mathrm{E}\left[(Z_{k+1} - Z_k)^2\right]$ may be recast as the variance of the integral of the point process under study multiplied by the following function:

$$\psi_{\mathrm{Haar}}(t) = \begin{cases} -1 & \text{for } -T < t < 0, \\ +1 & \text{for } 0 < t < T, \\ 0 & \text{otherwise.} \end{cases} \tag{16}$$

Equation (16) defines a scaled wavelet function, specifically the Haar wavelet. This can be generalized to any admissible wavelet $\psi(t)$; when suitably normalized, the result is a wavelet Allan

factor (WAF).[86,87] This generalization enables an increased range of fractal exponents to be estimated, at the cost of reducing the range of times over which the WAF varies as $T^{\alpha}$. In particular, for a particular wavelet with regularity (number of vanishing moments) $R$, fractal exponents $\alpha < 2R+1$ can be reliably estimated.[86,87] For the Haar basis, $R = 1$, while all other wavelet bases have $R > 1$. Thus the WAF employing bases other than the Haar should prove useful in connection with FRSPPs for which $\alpha \geq 3$; for processes with $\alpha < 3$, however, the AF appears to be the best choice.[86,87]

### 3.7 Relationships Among the Measures

For an ideal FSPP or FRSPP with $0 < \alpha < 1$, any one of Eqs. (8), (9), (12), and (15) implies the other three, with[2,88]

$$\begin{aligned} \lambda\tau_0^{1-\alpha}T_0^{\alpha} &= \alpha(\alpha+1)/2 \\ \omega_0^{\alpha}T_0^{\alpha} &= \cos(\pi\alpha/2)\Gamma(\alpha+2) \\ T_0^{\alpha}T_1^{-\alpha} &= 2-2^{\alpha}\,. \end{aligned} \tag{17}$$

For larger values of $\alpha$, the FF and CR do not scale, although the PSD and AF do; thus Eqs. (9), and (15) imply each other for these FRSPPs. Therefore, over the range of $\alpha$ for which the AF exhibits scaling[88]

$$\omega_0^{\alpha}T_1^{\alpha} = \begin{cases} \cos(\alpha\pi/2)\Gamma(2+\alpha)/(2-2^{\alpha}) & \text{for } 0<\alpha<1 \\ \pi/\ln(4) & \text{for } \alpha = 1 \\ -\cos(\alpha\pi/2)\Gamma(2+\alpha)/(2^{\alpha}-2) & \text{for } 1<\alpha<3\,. \end{cases} \tag{18}$$

In principle, any of the these statistics could be solved for $\alpha$ when it is known that $\alpha < 1$, although best results obtain from the PG and the AF.

Since the GD of a fractal cannot exceed the Euclidean dimension, which assumes a value of unity for one-dimensional point processes, FSPPs cannot exist for $\alpha > 1$; only FRSPPs are possible at these values of the fractal exponent.

## 4. SYNTHESIS OF FRACTAL AND FRACTAL-RATE STOCHASTIC POINT PROCESSES

In previous work we defined an FSPP and several FRSPPs and derived a number of their statistics.[2,23,89] We include brief summaries of these here, as well as of the clustered Poisson point-process model of Grüneis and colleagues.[90] We also introduce two new fractal-rate processes (fractal lognormal noise and fractal exponential noise) and define two new methods for generating point processes from a rate function: integrate-and-fire and controlled variability integrate-and-fire. These prove useful in isolating the effects of fractal components from those of nonfractal noise introduced through the mechanics of generating the point process. For all of the processes considered, the scaling relation in Eq. (2) holds for a number of statistical measures.

### 4.1 Fractal Renewal Point Process (FRP)

The one-dimensional homogeneous Poisson point process (HPP) is perhaps the simplest nonfractal stochastic point process.[91] The HPP is characterized by a single constant quantity, its rate, which is the number of events expected to occur in a unit interval. A fundamental property of the HPP is that it is memoryless; given this rate, knowledge of the entire history and future of a given realization of a HPP yields no information about the behavior of the process at the present. The HPP belongs to the class of renewal point processes; times between events are independent and identically distributed. The HPP is the particular renewal point process for which this distribution follows a decaying exponential form.

We now turn to a renewal process that is fractal: the standard fractal renewal process (FRP).[23,24,27,28,41] In the standard FRP, the times between adjacent events are independent random variables drawn from the same fractal probability distribution. In particular, the interevent-interval probability density function $p(t)$ decays essentially as a power law function

$$p(t) = \begin{cases} k/t^{\alpha+1} & \text{for } A < t < B \\ 0 & \text{otherwise}\,, \end{cases} \tag{19}$$

where $\alpha$ is the fractal exponent, $A$ and $B$ are cutoff parameters, and $k$ is a normalization constant. The FRP exhibits fractal behavior over time scales lying between $A$ and $B$. This process is fully fractal for $0 < \alpha < 1$: the power spectral density, coincidence rate, Fano factor, Allan factor, and even the interevent-time survivor function all exhibit scaling

as in Eq. (2) with the same power-law exponent $\alpha$ or one simply related to it.

Further, for this process the capacity or box-counting dimension $D_0$ assumes the value $\alpha$;[23] since the FRP is ergodic, the generalized fractal dimension $D_q$ becomes independent of the index $q$,[81] so $D_q = D_0 = \alpha$ for all $q$, and all fractal dimensions coincide.

A different (nonrenewal) point process results from the superposition of a number $K$ of independent FRPs; however, for this combined process as $K$ becomes large, and indeed for any FRSPP, the interevent-time probability density function no longer scales, and the generalized dimensions $D_q$ no longer equal $\alpha$, although the PG and AF (and the FF and CR, for $0 < \alpha < 1$) retain their scaling behavior. As the number of such processes increases, and for certain ranges of parameters, this superposition ultimately converges to the fractal Gaussian-noise driven Poisson process[23,41] (see also Secs. 4.2.1 and 4.4).

The standard FRP described above is a point process, consisting of a set of points or marks on the time axis as shown in Fig. 5(a); however, it may be recast as a real-valued process which alternates between two values, for example zero and unity. This alternating FRP would then start at a value of zero (for example), and then switch to a value of unity at a time corresponding to the first event in the standard FRP. At the second such event in the standard FRP, the alternating FRP would switch back to zero, and would proceed to switch back and forth at every successive event of the standard FRP. Thus the alternating FRP is a Bernoulli process, with times between transitions given by the same interevent-interval probability density as in the standard FRP, as portrayed in Fig. 5(b).

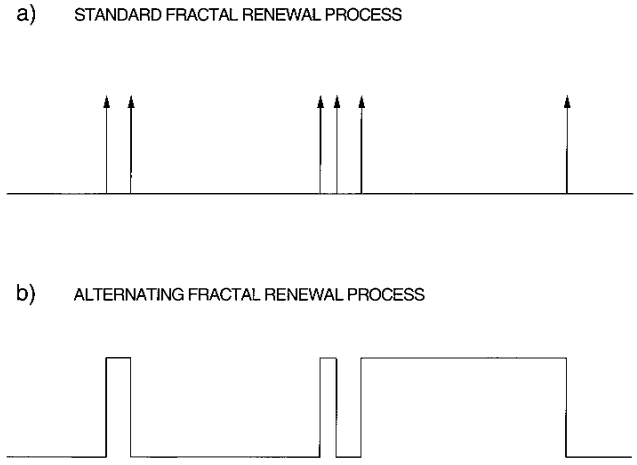


**Fig. 5** Sample functions of fractal renewal processes. Interevent times are power-law distributed. **(a)** The standard fractal renewal process (FRP) consists of Dirac $\delta$ functions and is zero-valued elsewhere. **(b)** The alternating FRP switches between values of zero and unity.

## 4.2 Integrate-and-Fire Fractal-Rate Stochastic Point Processes

Many point processes derive from a continuous-time function $\lambda(t)$ which serves as the stochastically varying rate of the point process. These are known as fractal-rate stochastic processes (FRSPPs). We confine our discussion to rate processes (and therefore FRSPPs) which are ergodic. Perhaps the simplest means for generating a point process from a rate is the integrate-and-fire (IF) method.[76] In this model, the rate function is integrated until it reaches a fixed threshold $\theta$, whereupon a point event is generated and the integrator is reset to zero. Thus the occurrence time of the $(k+1)$st event is implicitly obtained from the first occurrence of

$$\int_{t_k}^{t_{k+1}} \lambda(t)\, dt = \theta\,. \tag{20}$$

With such a direct conversion from the rate process to the point process, any measure applied to these point processes will return results closely related to the fractal structure of the underlying rate process $\lambda(t)$. In particular, over small frequencies, the theoretical PSDs of the rate process and of the resulting point process coincide.

We now turn to methods for generating several different kinds of fractal rate functions. More complex methods for point-process generation, as delineated in Secs. 4.3 and 4.4, can also be applied to these same rate functions.

### 4.2.1 *Fractal Gaussian Noise (FGN)*

Gaussian processes are ubiquitous in nature and are mathematically tractable. The values of these processes at any number of fixed times form a jointly Gaussian random vector; this property, the mean, and the spectrum completely define the process. For use as a rate process, we choose a stationary

process with a mean equal to the expected rate of events, and a spectrum of the form of Eq. (9) with cutoffs. FGN properly applies only for $\alpha < 1$; the range $1 < \alpha < 3$ is generated by fractal Brownian motion.[5] However, in the interest of simplicity, we employ the term fractal Gaussian noise for all values of $\alpha$. A number of methods exist for generating FGN[8,92–94] typically the result is a sampled version of FGN with equal spacing between samples. Interpolation between these samples is usually achieved by selecting the most recently defined value.

With a rate process described by FGN serving as the input to an IF process, the fractal-Gaussian-noise driven integrate-and-fire process (FGNIF) results. Generally, we require that the mean of the rate process be much larger than its standard deviation, so that the times when the rate is negative (during which no events may be generated) remain small. The FGNIF has successfully been used to model the human heartbeat[75,76] (see Sec. 2.9).

All of the rate processes considered in the following subsections converge to FGN under appropriate circumstances, and thus the point processes they yield through the IF construct converge to the FGNIF.

### 4.2.2 *Fractal Lognormal Noise (FLN)*

A related process results from passing FGN through a memoryless exponential transform. Since the exponential of a Gaussian is lognormal, we call this process fractal lognormal noise (FLN). If $X(t)$ denotes an FGN process with mean $\mathrm{E}[X]$, variance $\mathrm{Var}[X]$, and autocovariance function $K_X(\tau)$, then $\lambda(t) \equiv \exp[X(t)]$ is an FLN process with moments $\mathrm{E}[\lambda^n] = \exp\{n\mathrm{E}[X] + n^2\mathrm{Var}[X]/2\}$ and autocovariance function $K_\lambda(\tau) = \mathrm{E}^2[\lambda]\{\exp[K_X(\tau)] - 1\}$.

When this rate serves as the input to a doubly stochastic Poisson point process (see Sec. 4.4), the result provides an excellent model for vesicular exocytosis (see Sec. 2.4). By virtue of the exponential transform, the autocorrelation functions of the Gaussian process $X(t)$ and the lognormal process $\lambda(t)$ differ; thus their spectra differ. In particular, the PSD of the resulting point process does not follow the exact form of Eq. (9), although for small values of $\mathrm{Var}[X]$, as encountered in modeling exocytosis (for which $\mathrm{Var}[X] \leq 0.6$),[46,47] the experimental PG closely resembles this ideal form. In the limit of very small $\mathrm{Var}[X]$, the exponential operation approaches a linear transform, and the rate process becomes FGN.

### 4.2.3 *Fractal Exponential Noise (FEN)*

Other nonlinear transforms may be applied to FGN, yielding other fractal rate processes; we consider one which generates an exponentially distributed process. If $X_1(t)$ and $X_2(t)$ denote two independent and identically distributed FGN processes with zero mean, variance $\mathrm{Var}[X]$, and autocovariance function $K_X(\tau)$, then $\lambda(t) \equiv X_1^2(t) + X_2^2(t)$ is a fractal exponential noise (FEN) process with moments $\mathrm{E}[\lambda^n] = 2^n n!\,(\mathrm{Var}[X])^n$ and autocovariance function $K_\lambda(\tau) = 4K_X^2(\tau)$. The rate $\lambda(t)$ turns out to be exponentially distributed. If $K_X(\tau)$ scales as in Eq. (8) with an exponent $\alpha_X$ in the range $1/2 < \alpha_X < 1$, then so will $K_\lambda(\tau)$, but with an exponent $\alpha_\lambda = 2\alpha_X - 1$.

This process may prove useful in the study of certain kinds of thermal light.[95] Such light has an electric field which comprises two independent components, with Gaussian amplitude distributions. The light intensity is the sum of the squares of the two fields, and therefore has an exponential amplitude distribution.

### 4.2.4 *Fractal Binomial Noise (FBN)*

A number of independent, identical alternating fractal renewal processes (see Sec. 4.1) may be added together, yielding a binomial process with the same fractal exponent as each individual alternating FRP.[23] This binomial process can serve as a rate process for an integrate-and-fire process; the fractal-binomial-noise driven integrate-and-fire (FBNIF) results. It is schematized in Fig. 6. As the number of constituent processes increases, the FBN rate converges to FGN (see Sec. 4.2.1) with the same fractal exponent.

### 4.2.5 *Fractal Shot Noise (FSN)*

Though the HPP itself is not fractal, linearly filtered versions of it, denoted shot noise, can exhibit fractal characteristics. In particular, if the impulse response function of the filter has a decaying power-law (fractal) form, the result is fractal shot noise

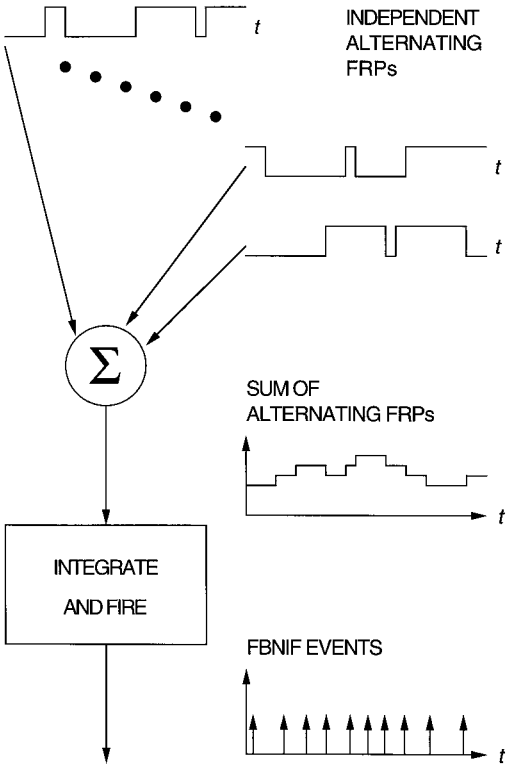


**Fig. 6** A sum of several independent and identical alternating FRPs (*top*) are added (*center*) to produce a fractal binomial noise process which serves as the rate function for an integrate-and-fire point process (*bottom*). The result is the fractal-binomial-noise-driven integrate-and-fire point process (FBNIF).

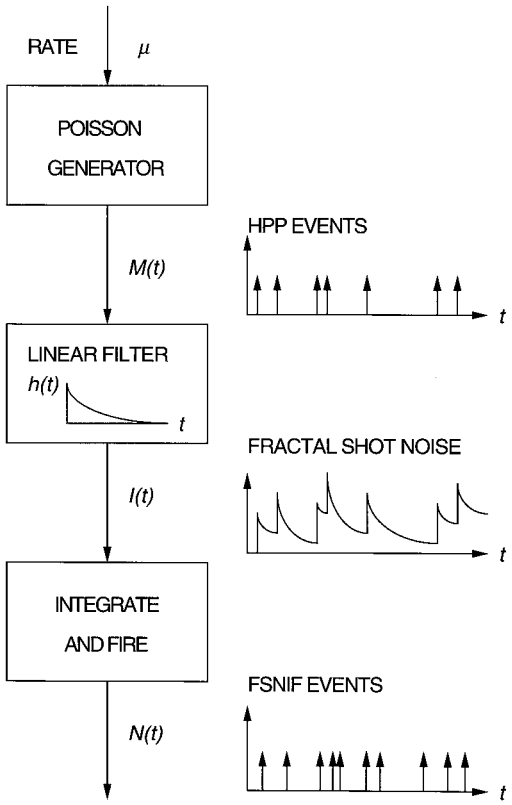


**Fig. 7** A primary homogeneous Poisson point process $M(t)$ with constant rate $\mu$ serves as the input to a linear filter with impulse response function $h(t)$. The continuous-time stochastic process $I(t)$ at the output of this filter is shot noise, which serves as the random rate for an integrate-and-fire process whose output is $N(t)$. $N(t)$ is the shot-noise driven integrate-and-fire point process (SNIF). If $h(t)$ decays in a power-law fashion, then $I(t)$ is fractal shot noise and $N(t)$ is a fractal SNIF or FSNIF.

(FSN).[96–98] If FSN serves as the rate for an IF process, the fractal-shot-noise driven integrate-and-fire process (FSNIF) results; Fig. 7 schematically illustrates the FSNDP as a two-stage process. The first stage produces a HPP with constant rate $\mu$. Its output $M(t)$ becomes the input to a linear filter with a power-law decaying impulse response function

$$h(t) = \begin{cases} k/t^{1-\alpha/2} & \text{for } A < t < B \\ 0 & \text{otherwise,} \end{cases} \tag{21}$$

where $\alpha$ is a fractal exponent between zero and two, $A$ and $B$ are cutoff parameters, and $k$ is a normalization constant. This filter produces fractal shot noise $I(t)$ at its output, which then becomes the time-varying rate for the last stage, an integrate-and-fire process. The resulting point process $N(t)$ reflects the variations of the fractal-shot-noise driving process. Under suitable conditions, FSN converges to FGN as provided by the central limit theorem;[98] the result is then the FGNIF.

## 4.3 Controlled-Variability Integrate-and-Fire Fractal-Rate Stochastic Point Processes

FRSPPs based on an integrate-and-fire substrate have only one source of randomness, which is the rate process $\lambda(t)$. Those based on a Poisson-process substrate (see Sec. 4.4) have a second source which depends explicitly on the rate process. We now generalize the family of FRSPPs to include those which have a second source of randomness that may be specified independently of the first. This new process differs from the simple IF process based on $\lambda(t)$, by the imposition of a specific form of jitter on the interevent times. After generating the time of the $(n+1)$st event $t_{n+1}$ in accordance with Eq. (20), the $(n+1)$st interevent time, $t_{n+1} - t_n$, is multiplied by

a Gaussian-distributed random variable with unit mean and variance $\sigma^2$. Thus $t_{n+1}$ is replaced by

$$t_{n+1} + \sigma(t_{n+1} - t_n)\mathcal{N}(0,1)\,, \tag{22}$$

where $\mathcal{N}(0,1)$ is a zero-mean, unity-variance Gaussian random variable. The result is the jittered-integrate-and-fire (JIF) family of processes. Employing the fractal-rate functions delineated in Sec. 4.2 yields the fractal-Gaussian-noise driven jittered-integrate-and-fire process (FGNJIF) (Sec. 4.2.1), the fractal-lognormal-noise driven jittered-integrate-and-fire process (FLNJIF) (Sec. 4.2.2), the fractal-exponential-noise driven jittered-integrate-and-fire process (FENJIF) (Sec. 4.2.3), the fractal-binomial-noise driven jittered-integrate-and-fire process (FBNJIF) (Sec. 4.2.4), and the fractal-shot-noise driven jittered-integrate-and-fire process (FSNJIF) (Sec. 4.2.5).

In these point processes, the standard deviation $\sigma$ of the Gaussian jitter is a free parameter that controls the strength of the second source of randomness. Two limiting situations exist. In the limit $\sigma \to 0$ the second source of randomness is absent and the JIF processes reduce to the simple IF process considered in Sec. 4.2. The opposite limit, $\sigma \to \infty$ leads to a homogeneous Poisson process; none of the fractal behavior in the rate process appears in the point process, as if the rate were constant. Between these two limits, as $\sigma$ increases from zero, the fractal onset times of the resulting point processes increase, and the fractal characteristics of the point processes are progressively lost, first at higher frequencies (shorter times) and subsequently at lower frequencies (longer times).

Finally, we note that another generalization of the integrate-and-fire formalism is possible.[76] The threshold for firing $\theta$ need not remain constant, but can itself be a random variable or stochastic process. Randomness imparted to the threshold can then be used to represent variability in other elements of a system, such as the amount of neurotransmitter released per exocytic event or the duration of ion channel openings. The homogeneous Poisson process (HPP) with rate $\lambda_0$ would then form a special case within this construct, generated when the rate is fixed and constant at $\lambda(t) = \lambda_0$, and $\theta$ is an independent, exponentially distributed unit mean random variable associated with each interevent interval. If the rate process $\lambda(t)$ is also random, a doubly stochastic Poisson point process results instead of the HPP.

### 4.4 Fractal-Rate Doubly Stochastic Poisson Point Process (FRDSPP)

We have seen that an integrate-and-fire process (with or without jitter) converts a fractal rate process into an FRSPP. A Poisson process substrate may be employed instead of the IF substrate, in which case the outcome is the family of doubly stochastic Poisson point processes (DSPPs).[99] DSPPs display two forms of randomness: one associated with the stochastically varying rate, and the other associated with the underlying Poisson nature of the process even if the rate were fixed and constant. With fractal rate processes, a fractal-rate DSPP (FRDSPP) results.[2] Again, simple relations exist between measures of the rate $\lambda(t)$ and the point process $dN(t)$. In particular, for the theoretical PSDs we have

$$S_N(\omega) = \mathrm{E}[\lambda] + S_\lambda(\omega)\,, \tag{23}$$

where $S_N(\omega)$ is the PSD of the point process and $S_\lambda(\omega)$ is the PSD of the rate.

As with the fractal IF processes considered above, the amount of randomness introduced by the second source in fractal DSPPs (the Poisson transform) may also be adjusted. However, in this case the amount introduced depends explicitly on the rate $\lambda(t)$, rather than being independent of it as with the JIF family of FRSPPs. For example, for a particular rate function $\lambda(t)$ suppose that its integral between zero and $t$ assumes the value $\Lambda$:

$$\int_0^t \lambda(u)\,du = \Lambda\,. \tag{24}$$

Then given $\Lambda$, the number of events $N(t)$ generated in the interval $(0,t]$ has a Poisson distribution, and in particular the mean and variance of $N(t)$ both assume a value of $\Lambda$. Therefore, if $\lambda(u)$ is multiplied by a constant value, then for a fixed integration time $t$, the mean and variance of $N(t)$ will change by the same factor. As this constant value increases, the coefficient of variation (the standard deviation divided by the mean) of

$N(t)$ decreases, and the contribution of the Poisson transform to the total randomness of the point process decreases, ultimately becoming negligible as the multiplication constant increases without limit. However, the DSPP formalism is less flexible than the JIF formalism for introducing randomness, since in the former case it explicitly depends on the mean number of events, while in the latter case the variance may be independently adjusted with the parameter $\sigma$.

Again, a variety of fractal point processes exist in the FRDSPP class, depending on the rate process chosen. Examples include the fractal-Gaussian-noise driven Poisson point process (FGNDP) (Sec. 4.2.1,[89]), the fractal-lognormal-noise driven Poisson point process (FLNDP) (Sec. 4.2.2,[46,47]), the fractal-exponential-noise driven Poisson point process (FENDP) (Sec. 4.2.3), the fractal-binomial-noise driven Poisson point process (FBNDP) (Sec. 4.2.4,[23,2]), and the fractal-shot-noise driven Poisson point process (FSNDP) (Sec. 4.2.5,[89]). For the FGNDP a slight modification is necessary since a negative rate has no meaning for a Poisson point process. Therefore, rather than using a Gaussian process directly we instead set the rate to zero for negative values of this process. We require that the mean rate be much larger than its standard deviation, so that the effect of this nonlinear limiting can essentially be ignored. Again, all forms of FRSPPs with positive finite mean rates converge to the FGNDP under appropriate conditions.[2]

### 4.5 Cluster Poisson Point Process

Other important formulations for FRSPPs exist. Grüneis and colleagues defined a clustered Poisson point process in which each member of a sequence of primary events from an HPP gives rise to a train of secondary events (as in the FSNDP), but where the events in the train form a segment of a renewal process (usually also an HPP, but often with a different rate), with a fractal (power-law distributed) duration.[100,90] The resulting process indeed exhibits power-law scaling in the same statistics as other FRSPPs.[101] The cluster Poisson point process is therefore a Bartlett–Lewis-type process, whereas the FSNDP is a process of the Neyman–Scott type.[1] This process has been used successfully to model mesencephalic reticular formation neural spike trains[70] (see Sec. 2.8).

## 5. ESTIMATION OF THE ALLAN FACTOR AND POWER SPECTRAL DENSITY: THEORY

Given a segment of an FRSPP, we seek an estimate $\widehat{\alpha}$ of the true fractal exponent $\alpha$ of the entire process from which the segment was derived. Several effects contribute to estimation error for finite-length segments, regardless of the method used. The fractal exponent provides a measure of the relative strengths of fluctuations over various time scales; for an FRSPP with a relatively large fractal exponent, for example, relatively more energy is concentrated in longer time scale fluctuations than for an FRSPP with a smaller fractal exponent. Variance stems from the inherent randomness of the strengths of these fluctuations. A collection of finite realizations of an FRSPP with the same parameters will exhibit fractal fluctuations of varying strengths, leading to a distribution of estimated fractal exponents.

Bias appears to arise from cutoffs in the time (frequency) domain which give rise to oscillations in the frequency (time) domain, confounding the pure power-law behavior of the fractal PG (AF). In addition, the physical limitations of the measurement process itself impose practical limits on the range of time scales available. Although algorithms exist for accurately compensating for these cutoffs, they presuppose a detailed knowledge of the process *a priori*, which is not in the spirit of estimating an unknown signal. Consequently, in this paper we do not attempt to compensate for these cutoffs in this manner. In previous work[2] we determined the theoretical expected Fano factor values for an FRSPP with finite duration, and the corresponding expected bias for the corresponding fractal exponent. Bias for the power spectral density was also considered, but not for a finite data length.

The AF and the PG highlight the fractal behavior of FRSPPs particularly well, and thus prove to be most useful for estimating fractal exponents, as indicated in Sec. 3. We proceed to investigate the bias in these measures, and the effects of this bias on fractal-exponent estimation. The variance

of PG-based estimators was examined previously;[2] that for the AF appears not to be readily amenable to analytical study.

### 5.1 Effects of Finite Data Length on the AF Estimate

Unlike the Fano factor, estimates of the AF do not suffer from bias due to finite data length; thus fractal exponent estimates based on the AF do not either. Given a particular data set, the estimated AF $\widehat{A}(T)$ at a particular counting time $T$ is given by

$$\widehat{A}(T) = (N-1)^{-1} \sum_{k=0}^{N-2} (Z_{k+1} - Z_k)^2 \Big/ 2N^{-1} \sum_{k=0}^{N-1} Z_k \,, \tag{25}$$

where $N$ is the number of samples, $\{Z_k\}$ represents the sequence of counts as shown in Fig. 1(c), and the functional dependence of $Z_k$ upon $T$ is suppressed for notational clarity.

This estimate of the AF is simply the estimate of the Allan variance divided by twice the estimate of the mean; however, computing the expected value of this estimate is not straightforward. We therefore employ the true mean rather than its estimate in Eq. (25). This does not appreciably affect the result, since the error so introduced remains a constant factor for all counting times, and so cancels in power-law slope calculations where logarithms are used. In any case, the estimate of the Allan variance exhibits far larger variations than the estimate of the mean, so the fluctuations in the AF estimate are dominated by the former. Therefore, the expected value of the AF estimate becomes

$$\begin{aligned} \mathrm{E}\left[\widehat{A}(T)\right] &= \mathrm{E}\left\{ \widehat{\mathrm{E}}\left[(Z_k - Z_{k+1})^2\right] \Big/ 2\widehat{\mathrm{E}}[Z_k] \right\} \\ &\approx \mathrm{E}\left[(Z_k - Z_{k+1})^2\right] \Big/ 2\mathrm{E}[Z_k] \\ &= \mathrm{E}\left[(Z_0 - Z_1)^2\right] \Big/ 2\mathrm{E}[Z_0] \\ &= (\lambda T)^{-1} \mathrm{E}\left[Z_0^2 - Z_0 Z_1\right] \,, \end{aligned} \tag{26}$$

which is independent of the number of samples, $N$, and therefore of the duration of the recording $L$. In the limit $L \to \infty$, the expected estimated AF for an FRSPP with $0 < \alpha < 3$ follows the form of Eq. (15) precisely, by definition of an ergodic process. Since Eq. (26) does not depend on $L$, the quantity $\mathrm{E}\left[\widehat{A}(T)\right]$ must assume a constant value independent of $L$; thus the AF does not exhibit bias caused by finite data duration. Finally, since the expected value of the AF estimate is unbiased, the expected value of the estimate of $\alpha$ itself is expected to have negligible bias. This is a simple and important result.

Estimates of the ordinary variance and Fano factor, in contrast, do depend on the duration. In this case we have

$$\begin{aligned} \widehat{\mathrm{Var}}[Z] &= (N-1)^{-1} \sum_{k=0}^{N-1} (Z_k - \widehat{\mathrm{E}}[Z])^2 \\ &= (N-1)^{-1} \sum_{k=0}^{N-1} \left( Z_k - N^{-1} \sum_{l=0}^{N-1} Z_l \right)^2 \\ &= (N-1)^{-1} \left[ \sum_{k=0}^{N-1} Z_k^2 - 2N^{-1} \sum_{k=0}^{N-1} \sum_{l=0}^{N-1} Z_k Z_l \right. \\ &\quad \left. + N^{-2} \sum_{k=0}^{N-1} \sum_{l=0}^{N-1} \sum_{m=0}^{N-1} Z_l Z_m \right] \\ &= (N-1)^{-1} \sum_{k=0}^{N-1} Z_k^2 \\ &\quad - N^{-1}(N-1)^{-1} \sum_{k=0}^{N-1} \sum_{l=0}^{N-1} Z_k Z_l \\ &= N^{-1} \sum_{k=0}^{N-1} Z_k^2 - N^{-1}(N-1)^{-1} \sum_{k=0}^{N-1} \sum_{l \neq k} Z_k Z_l \,. \end{aligned} \tag{27}$$

These cross terms, which do depend on the number of samples, lead to an estimated Fano factor with a confounding linear term

$$\mathrm{E}\left[\widehat{F}(T)\right] \approx 1 + (T/T_0)^{\alpha} - T \Big/ \left(T_0^{\alpha} L^{1-\alpha}\right) \tag{28}$$

for $0 < \alpha < 1$.[2] The last term on the right-hand-side of Eq. (28) leads to bias in estimating the fractal exponent; for this and other reasons, we do not employ the FF in fractal-exponent estimation.

### 5.2 Effects of Finite Data Length on the PSD Estimate

Computation of the periodogram (estimated PSD) proves tractable only when obtained from the series of counts $\{Z_k\}$, rather than from the entire point

process $N(t)$. This, and more importantly the finite length of the data set, introduce a bias in the estimated fractal exponent as shown below.

We begin by obtaining the discrete-time Fourier transform of the series of counts $\{Z_k\}$, where $0 \leq k < M$:

$$\tilde{Z}_n \equiv \sum_{k=0}^{M-1} Z_k e^{-j2\pi kn/M} \,. \tag{29}$$

The periodogram then becomes

$$\begin{aligned} \widehat{S}_Z(n) &= M^{-1} \left| \tilde{Z}_n \right|^2 \\ &= M^{-1} \sum_{k=0}^{M-1} \sum_{m=0}^{M-1} Z_k Z_m e^{j2\pi(k-m)n/M} \,, \end{aligned} \tag{30}$$

with an expected value

$$\begin{aligned} \mathrm{E}\left[\widehat{S}_Z(n)\right] &= M^{-1} \sum_{k=0}^{M-1} \sum_{m=0}^{M-1} e^{j2\pi(k-m)n/M} \mathrm{E}\left[Z_k Z_m\right] \\ &= M^{-1} \sum_{k=0}^{M-1} \sum_{m=0}^{M-1} e^{j2\pi(k-m)n/M} \mathrm{E}\left[\int_{s=0}^{T} \int_{t=0}^{T} dN(s+kT) dN(t+mT)\right] \\ &= M^{-1} \sum_{k=0}^{M-1} \sum_{m=0}^{M-1} e^{j2\pi(k-m)n/M} \int_{s=0}^{T} \int_{t=0}^{T} G_N[s-t+(k-m)T] \, ds \, dt \\ &= M^{-1} \sum_{k=0}^{M-1} \sum_{m=0}^{M-1} e^{j2\pi(k-m)n/M} \int_{u=-T}^{T} \int_{v=|u|}^{2T-|u|} G_N[u+(k-m)T] \, \frac{du \, dv}{2} \\ &= M^{-1} \sum_{k=0}^{M-1} \sum_{m=0}^{M-1} e^{j2\pi(k-m)n/M} \int_{u=-T}^{T} (T-|u|) \, G_N[u+(k-m)T] \, du \\ &= M^{-1} \sum_{k=0}^{M-1} \sum_{m=0}^{M-1} e^{j2\pi(k-m)n/M} \int_{u=-T}^{T} (T-|u|) \\ &\qquad \times \int_{\omega=-\infty}^{\infty} S_N(\omega) \, e^{j\omega[u+(k-m)T]} \, \frac{d\omega}{2\pi} \, du \\ &= (2\pi M)^{-1} \int_{\omega=-\infty}^{\infty} S_N(\omega) \left| \sum_{k=0}^{M-1} e^{jk(2\pi n/M+\omega T)} \right|^2 \int_{u=-T}^{T} (T-|u|) \, e^{j\omega u} \, du \, d\omega \\ &= (2\pi M)^{-1} \int_{\omega=-\infty}^{\infty} S_N(\omega) \frac{\sin^2(\pi n + M\omega T/2)}{\sin^2(\pi n/M + \omega T/2)} \frac{4\sin^2(\omega T/2)}{\omega^2} \, d\omega \\ &= \frac{T}{\pi M} \int_{-\infty}^{\infty} S_N(2x/T) \frac{\sin^2(Mx)\sin^2(x)}{x^2 \sin^2(x+\pi n/M)} \, dx \,. \end{aligned} \tag{31}$$

For a general fractal stochastic point process, where the PSD follows the form of Eq. (9), we therefore have

$$\mathrm{E}\left[\widehat{S}_Z(n)\right] = \frac{\lambda T}{\pi M} \int_{-\infty}^{\infty} \left[1 + (\omega_0 T/2)^{\alpha} |x|^{-\alpha}\right] \frac{\sin^2(Mx)\sin^2(x)}{x^2 \sin^2(x+\pi n/M)} \, dx \,. \tag{32}$$

Focusing on the smaller values of $n$ useful in estimating fractal exponents permits the use of two approximations in Eq. (32). For the values of $\alpha$ used in this paper ($0 < \alpha < 2$), the integrand of Eq. (32) will only

be significant near $x = -\pi n/M$, yielding

$$\begin{aligned}\mathrm{E}\left[\widehat{S}_Z(n)\right] &\approx \frac{\lambda T}{\pi M}\int_{-\infty}^{\infty}\left[1+(\omega_0 T/2)^{\alpha}|x|^{-\alpha}\right] \\ &\quad\times\frac{M\pi\delta(x+\pi n/M)\sin^2(x)}{x^2}\,dx \\ &= \lambda T\left[1+(2\pi n/\omega_0 MT)^{-\alpha}\right]\frac{\sin^2(\pi n/M)}{(\pi n/M)^2} \\ &\approx \lambda T\left[1+(2\pi n/\omega_0 MT)^{-\alpha}\right], \qquad (33)\end{aligned}$$

which is of the same form as Eq. (9). Improvement of this estimation procedure appears to require numerical integration of Eq. (32), which proves nontrivial since the integrand exhibits oscillations with a small period $\pi/M$. Fortuitously, for the parameter values employed in this paper the integrand appears peaked near $x = -\pi n/M$, so that not too many ($\approx 200$) oscillations need be included in the calculations. Indeed, numerical results employing this method, and with $\omega_0 \to 0$ for which Eq. (32) is known to assume the simple value $\lambda T$, agree within 0.1%. These results form an extension of earlier approaches[2,83] which ignored the effects of imposing periodic boundary conditions on the Fourier transform, and of binning the events. Numerical integration of Eq. (32) followed by a least-squares fit on a doubly logarithmic plot leads to results for the expected bias of the PSD-based estimate of the fractal exponent, shown in Table 2.

Other methods exist for compensating for finite data length in power spectral estimation, such as maximizing the entropy subject to the correlation function over the available range of times (see, e.g.,[102]).

## 6. ESTIMATION OF THE ALLAN FACTOR AND POWER SPECTRAL DENSITY: SIMULATION

Having considered various possible theoretical sources of error in simulating FRSPPs with a desired fractal exponent, we now proceed to investigate their effects upon fractal exponent estimates based on the power spectral density and Allan factor measures. To this end we employ simulations of three of the FRSPPs outlined above: FGN driving a deterministic integrate-and-fire process (FGNIF), FGN driving an IF process followed by Gaussian jitter of the interevent intervals (FGNJIF), and FGN driving a Poisson process (FGNDP). We choose these three processes from the collection presented in Sec. 4 for a number of reasons. First, the FGNIF, FGNJIF, and FGNDP derive from a common continuous-time rate process, fractal Gaussian noise (FGN), and thus differences among these point processes must lie in the point-process generation mechanism rather than in the fractal rate processes. Second, FGN admits fractal exponent of any value, while the fractal exponents cannot exceed two for fractal binomial noise and fractal shot noise. Third, of all the FRSPPs examined in Sec. 4, those based on the FGN appear to suffer the least from the effects of cutoffs, so that expected values of the PG and the AF most closely follow the pure power-law forms of Eqs. (9) and (15) respectively.

To generate the rate function with $1/f^{\alpha}$ spectral properties, we computed discrete-time approximations to fractal Gaussian noise (FGN) by forming a conjugate-symmetric sequence $\tilde{X}[k]$ of $M$ samples which satisfies

$$\left|\tilde{X}[k]\right| = \begin{cases} M\rho & \text{for } k = 0 \\ ck^{-\alpha/2} & \text{for } 1 \le k \le M/2\,, \end{cases} \qquad (34)$$

where $\rho = \mathrm{E}[\lambda(t)]$ is the desired average value of the FGN process, and $c$ is a constant determining the relative strength of the FGN. The phases of $\tilde{X}[k]$ were independent and uniformly distributed in the interval $[0, 2\pi)$ for $1 \le k < M/2$, while both $\tilde{X}[0]$ and $\tilde{X}[M/2]$ were strictly real. A discrete-time sequence $\tilde{x}[n]$ was obtained by taking the inverse discrete Fourier transform of $\tilde{X}[k]$. The resulting FGN process is periodic with period $M$, so to reduce the effects of this periodicity we employ only the first half of the sequence. Specifically, we used an original sequence $\tilde{x}[n]$ of length $M = 2^{16} = 65\,536$ points and kept the first $2^{15} = 32\,768$ samples as $x[n]$. Further, since rate functions must not attain negative values, we chose the mean value of the FGN, $\rho$, sufficiently large compared to the relative strength of the FGN $c$ to ensure that $x[n]$ remained positive for all $2^{15}$ different values of $x[n]$ in all simulations. In particular for $\alpha < 1$ this was adjusted by choosing the FF intercept time $T_0$ to be 10 times the average interevent time, while for $\alpha > 1$ the PSD fractal onset frequency $\omega_0$ was chosen to be 0.0005 times the average rate $\rho$.

The resultant sequence $x[n]$ was taken to represent equally spaced samples of a continuous-time process; to simplify subsequent analysis, we chose the duration of each sample to be one sec, without

loss of generality. Varying the mean event production rate $\rho$ while keeping all other parameters fixed (or in fixed relation to $\rho$, as with the FF intercept time and PSD corner frequency) resulted in point processes which contained varying expected numbers of events. In particular, we employed values of $\rho = 5, 10, 20, 40$ and 80 events per sample of $x[n]$, leading to a range of roughly 164 000 to 2 620 000 events in the resulting point process.

The following procedures were employed to compute the estimates described in Sec. 3. For the PG, the absolute event times were quantized into $2^{16}$ bins, which therefore formed a rate estimate of the process with counting windows having a duration of 0.5 sec. Then a discrete Fourier transform was performed, followed by replacing the Fourier components with their square magnitudes. Finally, a least-squares fit was performed on the logarithm of these quantities vs. the logarithm of the frequencies $f$ for various selected ranges of frequencies. These slopes form PG-based estimates of the fractal exponent.

Estimates of the AF were calculated over a range of counting times $T$ in a geometric sequence with ten counting times per decade. The slopes of the AF estimate were again obtained from linear least-squares fits to the logarithm of the AF values vs. the logarithm of the size of the counting time $T$; these slopes became the AF-based estimates of the fractal exponent. As indicated in Sec. 5.1, finite data lengths do not impart extraneous bias to the AF-based estimates.

For each type of FRSPP and value of $\rho$ employed, 100 simulations were performed for each of three different design values of the fractal exponent: $\alpha = 0.2$, 0.8, and 1.5; AF and PG curves were computed for each simulation. Estimates of the fractal exponent were obtained by two methods for each of these two measures. In the first, all 100 AF or PG curves were averaged together, after which the doubly logarithmic slope of this average curve was computed, yielding a single estimate of the fractal exponent. The second method consisted of first obtaining the doubly logarithmic slopes of the individual AF or PG curves, and then averaging these slopes. This second method yields the mean fractal exponent as well as the standard deviation (and other possible statistics of the fractal exponent).

As shown in Sec. 4.2, the FGN-driven integrate-and-fire process (FGNIF) is obtained by identifying the FGN sequence $x[n]$ as samples of a rate function $\lambda(t)$, taken to be constant over each sample of $x[n]$ (1 sec). This rate function is integrated until the result attains a value of unity, whereupon an output point is generated and the integrator is reset to zero. The generation of the continuous rate function from the piecewise-constant FGN does not significantly change the observed fractal structure of the resulting point process. For frequencies less than the inverse of the sampling time $T$ (1 Hz in this example), the PSDs of the piecewise-constant and exact versions of FGN differ by a factor of $\mathrm{sinc}^2(\omega T/2)$; fractal behavior depends on low frequencies ($\omega \ll 1/T$) where the above factor is essentially unity. Since the FGNIF process has just one source of randomness, namely the underlying FGN, the estimators for the fractal exponent should therefore display only the (fractal) behavior of the FGN itself, along with finite-size effects. Bias or variance due to a second source of randomness, such as the Poisson transform in the FGNDP, will not be present. Thus for our purposes the FGNIF process serves as a benchmark for the accuracy of fractal exponent estimators, with a bias and variance depending only on finite data size effects and not on the rate $\rho$.

The results for the FGNIF process with a rate $\rho = 40$ and three different fractal exponents ($\alpha$=0.2, 0.8 and 1.5) are summarized for the AF in Table 1 and for the PG in Table 2.

These Tables present estimated values of the fractal exponent $\widehat{\alpha}$ obtained from averages over 100 independent simulations, for a variety of time and frequency ranges. The exponents were obtained by the two methods delineated above, and are labeled "Fit of Avg." and "Avg. of Fits", respectively; theoretical results for the PSD are labeled "Theory". For an experimental AF or PG following the form of Eq. (15) or (9), respectively, the range of times or frequencies over which the fractal exponent is estimated will not significantly affect the returned value, as long as the range lies in the scaling region $\omega_0^{-1} \ll T \ll L$ (or $1/L \ll \omega \ll \omega_0$), respectively.

To demonstrate this, we estimated the fractal exponents over four time ranges (for the AF) and five frequency ranges (for the PG), with each range spanning a factor of ten or one hundred. As shown in Tables 1 and 2, the results for the averaged AF and PG curves do not depend significantly on the choice of fit ranges, and in general agree well with the design values of the fractal exponents $\alpha$. The deviations of the PG-based fractal exponent estimator from these design values are accounted for in part by the theoretical bias values obtained from the general result provided in Eq. (32), as shown in Table 2; these theoretical predictions yield the

**Table 1 AF-based fractal exponent estimates $\widehat{\alpha}$ for simulated FGNIF processes with a rate $\rho = 40$, for different time ranges. The governing rate processes have theoretical fractal exponents of $\alpha = 0.2$, 0.8, and 1.5. The estimated fractal exponents were obtained from straight-line fits on doubly logarithmic coordinates to an average curve of 100 independent simulations (Fit of Avg.) and from averages of the slopes of the individual curves (Avg. of Fits). The deviations are the standard deviations obtained from the second averaging procedure.**

| Range (sec.) | Method | $\alpha = 0.2$ | $\alpha = 0.8$ | $\alpha = 1.5$ |
|---|---|---|---|---|
| $62.5 - 625$ | Fit of Avg. | 0.199 | 0.799 | 1.499 |
| | Avg. of Fits | $0.194 \pm 0.074$ | $0.795 \pm 0.072$ | $1.495 \pm 0.067$ |
| $125 - 1250$ | Fit of Avg. | 0.211 | 0.807 | 1.499 |
| | Avg. of Fits | $0.199 \pm 0.119$ | $0.807 \pm 0.114$ | $1.490 \pm 0.105$ |
| $250 - 2500$ | Fit of Avg. | 0.219 | 0.804 | 1.490 |
| | Avg. of Fits | $0.184 \pm 0.165$ | $0.804 \pm 0.153$ | $1.472 \pm 0.138$ |
| $25 - 2500$ | Fit of Avg. | 0.204 | 0.801 | 1.495 |
| | Avg. of Fits | $0.192 \pm 0.056$ | $0.792 \pm 0.057$ | $1.487 \pm 0.059$ |

**Table 2 PG-based fractal exponent estimates $\widehat{\alpha}$ for simulated FGNIF processes with a rate $\rho = 40$, for different frequency ranges. The governing rate processes have theoretical fractal exponents of $\alpha = 0.2$, 0.8, and 1.5. The estimated fractal exponents were obtained from straight-line fits in doubly logarithmic coordinates to an average curve of 100 independent simulations (Fit of Avg.) and from averages of the slopes of the individual curves (Avg. of Fits). The deviations are the standard deviations obtained from the second averaging procedure. Also included are the theoretical bias values obtained from Eq. (32) and standard deviation values from [2, Eq. (17)]. These standard deviations are in substantial agreement with the data. Predictions of the bias underestimate the magnitude by factors of 3–10, although they correctly predict the sign.**

| Range (Hz) | Method | $\alpha = 0.2$ | $\alpha = 0.8$ | $\alpha = 1.5$ |
|---|---|---|---|---|
| $0.00025 - 0.0025$ | Fit of Avg. | 0.200 | 0.835 | 1.628 |
| | Avg. of Fits | $0.201 \pm 0.140$ | $0.836 \pm 0.137$ | $1.623 \pm 0.118$ |
| | Theory | $0.200 \pm 0.116$ | $0.807 \pm 0.116$ | $1.545 \pm 0.116$ |
| $0.0005 - 0.005$ | Fit of Avg. | 0.196 | 0.822 | 1.614 |
| | Avg. of Fits | $0.197 \pm 0.094$ | $0.823 \pm 0.093$ | $1.610 \pm 0.088$ |
| | Theory | $0.200 \pm 0.082$ | $0.804 \pm 0.082$ | $1.535 \pm 0.082$ |
| $0.001 - 0.01$ | Fit of Avg. | 0.202 | 0.821 | 1.605 |
| | Avg. of Fits | $0.202 \pm 0.078$ | $0.821 \pm 0.077$ | $1.602 \pm 0.075$ |
| | Theory | $0.200 \pm 0.058$ | $0.803 \pm 0.058$ | $1.526 \pm 0.058$ |
| $0.002 - 0.02$ | Fit of Avg. | 0.206 | 0.828 | 1.594 |
| | Avg. of Fits | $0.202 \pm 0.059$ | $0.824 \pm 0.057$ | $1.589 \pm 0.057$ |
| | Theory | $0.201 \pm 0.041$ | $0.802 \pm 0.041$ | $1.520 \pm 0.041$ |
| $0.0002 - 0.02$ | Fit of Avg. | 0.206 | 0.831 | 1.609 |
| | Avg. of Fits | $0.204 \pm 0.030$ | $0.830 \pm 0.031$ | $1.604 \pm 0.043$ |
| | Theory | $0.201 \pm 0.039$ | $0.803 \pm 0.039$ | $1.527 \pm 0.039$ |

correct sign for the bias, but underestimate the magnitude by factors of 3–10. Employing predictions directly based on the FGNIF process (see Appendix), rather than on a general FRSPP, yield results in substantial agreement with those of Eq. (32). The AF-based fractal exponent estimators, in contrast, do not suffer from bias due to finite data size, and thus agree with the design values directly. In particular, the AF yields better performance than the PG estimate, especially for the larger design fractal exponents values of $\alpha = 0.8$ and 1.5.

The fractal exponents computed by the second method are also listed in Tables 1 and 2, indicated by "Avg. of Fit", together with their standard deviations. (Note that for the first method there is no direct procedure to calculate the standard deviation since the results are extracted from a single curve). The two methods for estimating the fractal exponent agree remarkably well. For an ordinary Gaussian random variable, averaging over 100 samples would yield estimated values of the mean which exceeded the true mean by 2/10 of a standard deviation 5% of the time, with the rest clustered more tightly about the true mean. Of the 27 experiments in which both methods for estimating the fractal exponent were performed, for only one (AF, $\alpha = 0.2$, and $250 < T < 2500$) does the sample mean exceed this limit, suggesting that this simple Gaussian model is valid.

Useful estimators must have small variance as well as minimal bias; we therefore now focus on the standard deviations in Tables 1 and 2. For both the AF- and PG-based estimators, and for ranges spanning one decade, the standard deviation decreases slightly as the design values of the fractal exponent increase; for two-decade ranges, this trend is reversed. Standard deviations for the two-decade ranges are significantly less than those for a single decade, as expected. For ranges spanning one decade, the standard deviation increase with decreasing frequency (PG) or increasing counting time (AF); at these time and frequency scales, the PG has the worst proportional frequency resolution, and the AF suffers from relatively few counting windows over which to obtain accurate statistics. Finally, for similar time and frequency ranges the AF exhibits larger standard deviation than the PG. This is also likely due to the limited number of counting windows available, which proves more significant than the reduced resolution of the PG. Indeed, predictions of the estimated standard deviation for the PG based on earlier work[2] agree well with the data; these predictions in turn depend directly on the number of PG values available.

A figure of merit for fractal exponent estimators which combines the bias and variance is the root-mean-square error, equivalent to the square root of the sum of the variance and the squared bias. Employing the results for the individual AF and PG entries provided in Tables 1 and 2 yields the results shown in Table 3. For both the AF- and PG-based estimates, the best performance is associated with times and frequencies well away from the duration of the data set: smallest lower counting time limits for the AF, and largest upper frequency limits for the PG, respectively. Comparing conjugate time and frequency ranges shows that the fractal-exponent estimator based on the AF yields significantly superior performance for the largest design value of $\alpha$, while the PG proves somewhat better at the smallest value. Exact relationships between cutoff frequencies and cutoff times depend on the value of $\alpha$ itself[2] [see also Eq. (18)], so direct comparisons between ranges for the AF- and PG-based estimates vary among the columns of Table 3.

The results obtained are governed by the finite duration of the data and by the nature of the estimation process, and are not an artifact of the particular value of the rate, $\rho$, that was chosen. Reducing the rate from $\rho = 40$ to $\rho = 10$, while keeping all other parameters fixed, generates results which differ from those presented in Tables 1 and 2 by a maximum of $\pm 0.001$. Thus in the FGNIF, the integrate-and-fire algorithm appears to translate the fractal quality of the continuous FGN into a point process nearly perfectly. All differences between the estimated fractal exponents and the design values used in the generation of the FGNIF simulations must therefore be due to finite-size effects: bias for the PG-based estimator, as discussed in Sec 5.2, and variance for both PG- and AF-based estimators.

We now proceed to examine other point processes based on FGN, such as the FGNIF with jitter of the interevent intervals (FGNJIF) and the FGNDP. These processes, which include a second source of randomness that is inherent in the mechanism of point-process generation, exhibit increased fractal-exponent estimation error. We present averaged AF and PG plots for the FGNJIF with a mean rate $\rho = 10$ and jitter parameters $\sigma = 0$, 0.5, and 1 in Fig. 8. These plots attain asymptotic values at larger times (for the AF) and lower frequencies (PG) than those for the FGNIF do, especially for

**Table 3 Root-mean-square (rms) error of the estimated fractal exponent $\widehat{\alpha}$ for both AF- and PG-based estimators, for the same ranges and parameters used in Tables 1 and 2.**

| Statistic | Range | $\alpha = 0.2$ | $\alpha = 0.8$ | $\alpha = 1.5$ |
|---|---|---|---|---|
| AF | $62.5 - 625$ sec | 0.074 | 0.072 | 0.067 |
| | $125 - 1250$ sec | 0.119 | 0.114 | 0.105 |
| | $250 - 2500$ sec | 0.166 | 0.153 | 0.141 |
| | $25 - 2500$ sec | 0.057 | 0.058 | 0.060 |
| PG | $0.00025 - 0.0025$ Hz | 0.140 | 0.142 | 0.170 |
| | $0.0005 - 0.005$ Hz | 0.094 | 0.096 | 0.141 |
| | $0.001 - 0.01$ Hz | 0.078 | 0.080 | 0.127 |
| | $0.002 - 0.02$ Hz | 0.059 | 0.062 | 0.106 |
| | $0.0002 - 0.02$ Hz | 0.030 | 0.043 | 0.113 |

**Table 4 Fractal exponents estimated from the PG and AF of the FGNJIF process, with $\sigma$ chosen to be 0, 0.5, and 1. The governing rate processes have design fractal exponents of $\alpha = 0.2$, 0.8, and 1.5, and mean values of $\rho = 10$ in all cases. One hundred individual curves were averaged, after which a single exponent was computed. As $\sigma$ increases the estimators exhibit an increasingly negative bias.**

| Statistic | Range | Jitter $\sigma$ | $\alpha = 0.2$ | $\alpha = 0.8$ | $\alpha = 1.5$ |
|---|---|---|---|---|---|
| AF | $250 - 2500$ sec | 0 | 0.213 | 0.804 | 1.490 |
| | | 0.5 | 0.193 | 0.796 | 1.469 |
| | | 1 | 0.153 | 0.779 | 1.416 |
| PG | $0.002 - 0.02$ Hz | 0 | 0.206 | 0.828 | 1.594 |
| | | 0.5 | 0.189 | 0.796 | 1.104 |
| | | 1 | 0.143 | 0.718 | 0.649 |

larger values of the jitter parameter $\sigma$. This reduced range of scaling behavior serves to reduce the measured slopes of these curves and thus the estimated values of the fractal exponent for both the AF- and PG-based estimators, for all design values of $\alpha$ employed. For $\sigma = 0$, corresponding to zero jitter (the FGNIF), the slopes attain the values shown in Tables 1 and 2. Estimated fractal exponent values for the FGNJIF are presented in Table 4, which highlights the increasing negative bias for increased $\sigma$.

The AF curves in Fig. 8 exhibit two additional jitter-dependent features worthy of mention. First, as $\sigma$ increases the regularity of the signal decreases, leading to increased relative variance and a consequent decrease in the amplitude of the dip near $T = 1$ sec. Second, while the AF must approach an asymptotic value of unity for counting times $T$ less than half the minimum interevent interval [see Eqs. (13) and (14)], this does not appear to occur in Fig. 8 for $\sigma = 1$. This apparent conundrum is resolved by recognizing that large values of the jitter parameter $\sigma$ lead to an increased probability that two adjacent event times will be perturbed to new values very close to each other. Thus as $\sigma$ increases, the relative frequency of quite small interevent intervals also increases, and the AF must be extended to ever smaller counting times to approach its limit of unity. We chose not to plot the AF curves at these smaller counting times $T$, since our focus lies in fractal behavior, which manifests itself over longer time scales.

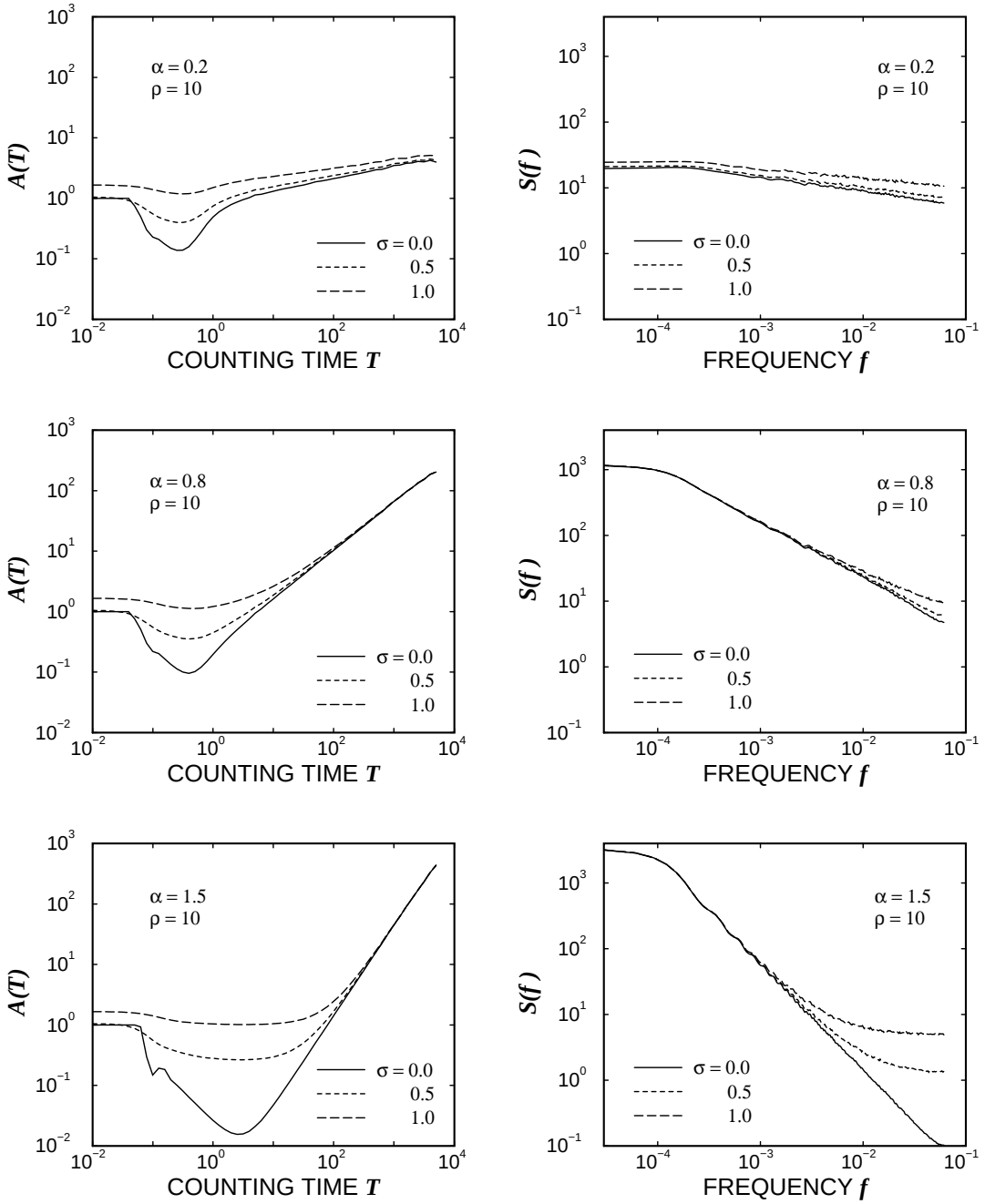


**Fig. 8** AF curves (*left*) and PG curves (*right*) of the fractal-Gaussian-noise driven integrate-and-fire process with jitter (FGNJIF), with $\sigma = 0$, 0.5, and 1 for three design values of the fractal exponent: $\alpha = 0.2$, 0.8, and 1.5. The mean rate $\rho = 10$ in all cases. The underlying rate function $x[n]$ consisted of $2^{15}$ samples, equally spaced at 1 sec each. For $\alpha = 0.2$ and $\alpha = 0.8$ the FF intercept time $T_0$ was 1 sec; for $\alpha = 1.5$ the PSD corner frequency $\omega_0$ was 0.005 Hz. Results from 100 simulations were averaged. The jitter reduces the range of scaling and systematically lowers the average slopes of the curves.

We now turn to the FGNDP, which has a Poisson-process substrate. As the average rate $\rho$ decreases, the relative contribution of the randomness introduced by the Poisson generator increases as $1/\sqrt{\rho}$, and the PG- and AF-based fractal-exponents estimators exhibit increasingly larger bias. We present results for simulated FGNDP processes in Fig. 9; Table 5 provides estimated fractal exponent values. The average differences between the estimated values of the fractal-exponents $\widehat{\alpha}$ and the design values $\alpha$ are shown graphically in Fig. 10 as a function of the mean event production rate $\rho$.

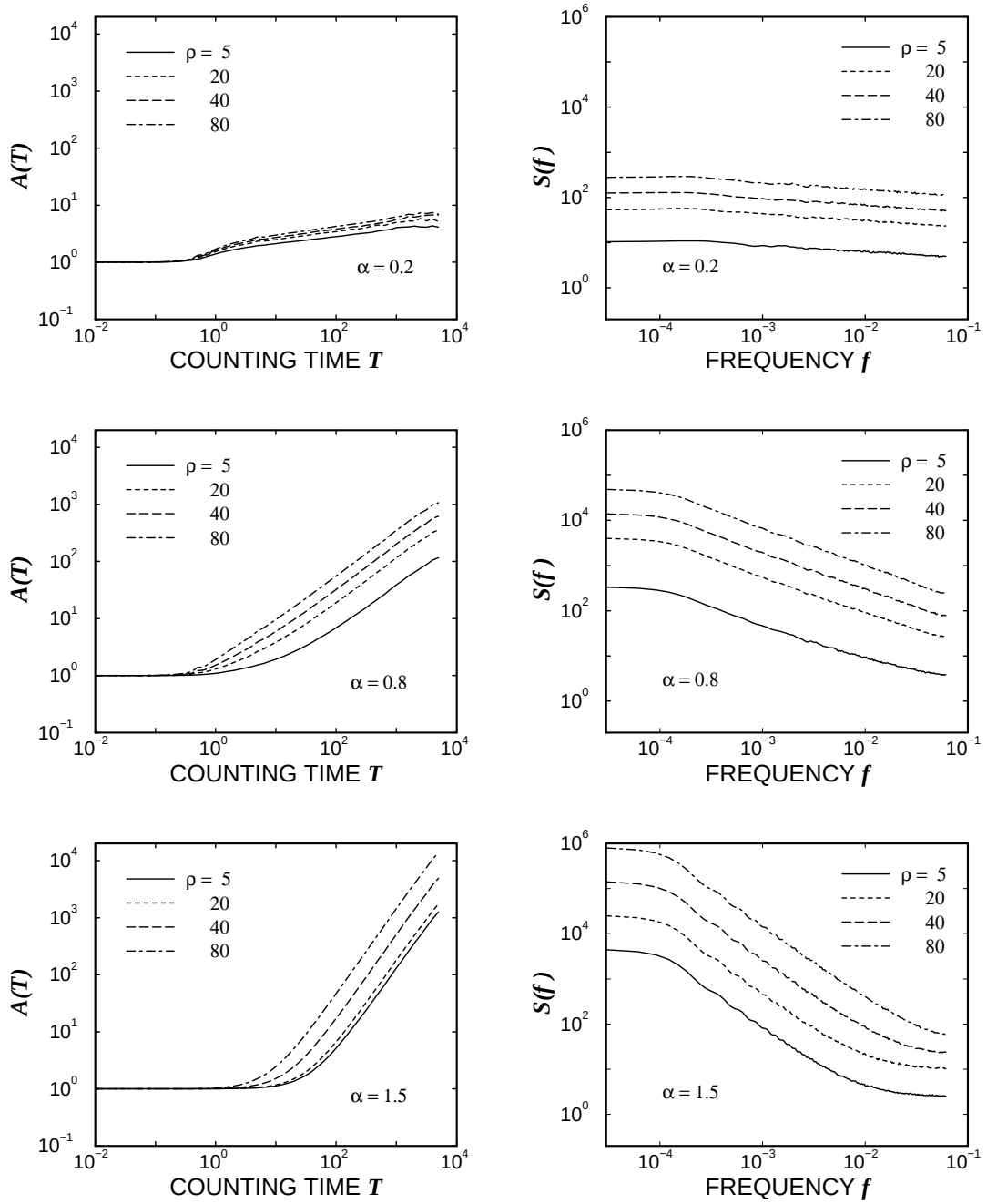


**Fig. 9** AF curves (*left*) and PG curves (*right*) of the fractal-Gaussian-noise driven Poisson process (FGNDP) with rate $\rho = 5$, 20, 40, and 80, for three design values of the fractal exponent: $\alpha = 0.2$, 0.8, and 1.5. The underlying rate function $x[n]$ consisted of $2^{15}$ samples, equally spaced at 1 sec each. For $\alpha = 0.2$ and $\alpha = 0.8$ the FF intercept time $T_0$ was 10 times the average interevent time $1/\rho$; for $\alpha = 1.5$ the PSD corner frequency $\omega_0$ was 0.0005 times the average rate $\rho$. Results from 100 simulations were averaged. As the rate decreases, the bias of the PG- and AF-based fractal exponent estimators increases.

For both the FGNJIF and the FGNDP processes, estimating fractal exponents over larger ranges of time or frequency leads to increased bias, particularly for large values of $\sigma$ and small values of $\rho$. Since the results depart from those obtained with the FGNIF, the additional randomness as $\rho$ decreases, or as $\sigma$ increases, leads to a dilution of the power-law behavior of the AF and PG, changing its onset to larger times and smaller frequencies. In the limits $\rho \to 0$ and $\sigma \to \infty$, the result is essentially white noise and the estimated fractal exponent will be zero.

**Table 5 Fractal exponents estimated from the PG and AF of the FGNDP process, with a rate $\rho$ chosen to be 5, 20, 40, and 80. The governing rate processes have design fractal exponents of $\alpha = 0.2$, 0.8, and 1.5. One hundred individual curves were averaged, after which a single exponent was computed. As $\rho$ decreases the estimators exhibit an increasingly negative bias.**

| Statistic | Range | Rate $\rho$ | $\alpha = 0.2$ | $\alpha = 0.8$ | $\alpha = 1.5$ |
|---|---|---|---|---|---|
| AF | $250 - 2500$ sec | 5 | 0.157 | 0.774 | 1.462 |
| | | 20 | 0.153 | 0.794 | 1.474 |
| | | 40 | 0.197 | 0.798 | 1.483 |
| | | 80 | 0.185 | 0.802 | 1.489 |
| PG | $0.002 - 0.02$ Hz | 5 | 0.130 | 0.652 | 0.997 |
| | | 20 | 0.132 | 0.764 | 1.092 |
| | | 40 | 0.149 | 0.786 | 1.351 |
| | | 80 | 0.157 | 0.804 | 1.496 |

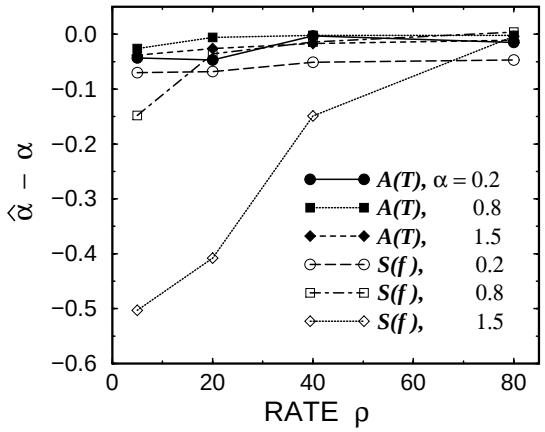


**Fig. 10** Average differences between the estimated values of the fractal exponents $\widehat{\alpha}$ and the design values $\alpha = 0.2$, 0.8, and 1.5 as a function of the mean event production rate $\rho$ for the fractal-Gaussian-noise driven Poisson process (FGNDP). The AF-based estimate yields smaller bias than the PG-based measure. For both fractal exponent estimators, bias decreases with increasing average rate $\rho$, especially for the PG-based estimator with $\alpha = 1.5$.

## 7. DISCUSSION

Best results for the FGNIF were obtained with the AF-based fractal-exponent estimator using counting times in the range $25 \leq T \leq 2500$; this yielded root-mean-square error results which were accurate to within 0.06 for all design values of $\alpha$ (Tables 1 and 3). For both the AF- and PG-based estimators, performance degraded at longer times and smaller frequencies (Tables 1, 2, and 3). Finite-duration effects in the PG and relatively few counting windows in the AF produce significant error over these scales. The rms error remained near 0.1 for both estimators, over all design values of the fractal exponent, and over all time and frequency ranges examined.

The FGNJIF and FGNDP processes impose a second source of randomness on the fractal behavior of the FGN kernel. This additional randomness is essentially uncorrelated, and thus may be modeled as the linear superposition of white noise on the original fractal signal; this affects the shapes of both the AF and the PG. As this white-noise level increases, it dilutes the fractal structure present in the FGN process, beginning at the shortest time scales and moving progressively towards longer ones. This effect reduces the range of times and frequencies over which fractal behavior appears, resulting in a decreased estimated fractal exponent. This proved most significant for larger design values of $\alpha$, and for the estimator based on the PG. Indeed, magnitudes of the bias exceeded 0.8 in one case. The AF-based estimator fared significantly better, although in this case it employed counting times which were five times the inverse of the frequencies used for the PG. These results compare favorably to earlier studies using the same number of events,[2] for which inaccuracies of 0.1 or larger were obtained for a variety of fractal stochastic point processes, all of which included a second source of randomness.

This study considered data sets with an average of $10^6$ points; experimental data may contain far fewer points, and thus yield poorer fractal-exponent estimation statistics. In particular, finite-size effects, which lead to increased bias for the PG-based estimator and increased variance for the AF-based estimator will reduce the ranges of times and frequencies over which reliable estimation can be achieved. Similarly, data sets with larger numbers of points (computer network traffic, for example) would yield superior performance. In addition, if several independent data sets are available, known to be from identical experiments, then the AF plots or the resulting estimates could be averaged, reducing the effective variance. In this case, the reduced bias in the AF-based estimator would render it far superior to that based on the PG.

Finally we mention that there exist several methods for reducing the bias of the fractal exponent estimates if one has some *a priori* knowledge of the process of interest. Such an approach however does not follow the philosophy of estimating a completely unknown signal and we therefore did not attempt to compensate for the bias by the use of such methods.

## 8. CONCLUSION

We have investigated the properties of fractal and fractal-rate stochastic point processes (FSPPs and FRSPPs), focusing on the estimation of measures that reveal their fractal exponents. The fractal-Gaussian-noise driven integrate-and-fire process (FGNIF) is unique as a point process in that it exhibits no short-term randomness; we have developed a generalization which includes jitter, the FGNJIF, for which the short-term randomness is fully adjustable. In addition to the randomness contributed by the fractal nature of the rate, all other FRSPPs appear to exhibit additional randomness associated with point generation, which confounds the accuracy of fractal-exponent estimation. The FGNJIF proved crucial in elucidating the role that such randomness plays in the estimation of fractal exponents in other FRSPPs. We presented analytical results for the expected biases of the PG- and AF-based fractional exponent estimators due to finite data length. We followed this theoretical work with a series of simulations of FRSPPs for three representative fractal exponents: $\alpha = 0.2$, 0.8, and 1.5. Using these simulations together with the analytical predictions, we delineated the sources of error involved in estimating fractal exponents. In particular, using the FGNJIF we were able to separate those factors intrinsic to estimation over finite FRSPP data sets from those due to the particular form of FRSPP involved. We conclude that the AF-based estimate proves more reliable in estimating the fractal exponent than the PG-based method, yielding rms errors of 0.06 for data segments of FRSPPs with $10^6$ points over all values of $\alpha$ examined. Finally, we note that wavelet generalizations of the AF appear to yield comparable results,[86,87] suggesting that the AF estimate may be optimal in some applications.

## 9. ACKNOWLEDGMENTS

We are grateful to M. Shlesinger for valuable suggestions. This work was supported by the Austrian Science Foundation under Grant No. S-70001-MAT (ST, MCF, HGF), by the Office of Naval Research under Grant No. N00014-92-J-1251 (SBL, MCT), by the Whitaker Foundation (SBL), and by the Joint Services Electronics Program through the Columbia Radiation Laboratory (MCT).

## REFERENCES

1. D. R. Cox and V. Isham, *Point Processes* (Chapman and Hall, London, 1980).
2. S. B. Lowen and M. C. Teich, "Estimation and Simulation of Fractal Stochastic Point Processes," *Fractals* **3**, 183-210 (1995).
3. W. Rudin, *Principles of Mathematical Analysis,* 3rd ed. (McGraw Hill, New York, 1976), p. 197.
4. M. F. Shlesinger and B. J. West, "Complex Fractal Dimension of the Bronchial Tree," *Phys. Rev. Lett.* **67**, 2106-2108 (1991).
5. B. B. Mandelbrot, *The Fractal Geometry of Nature* (W. H. Freeman, New York, 1983).
6. H. E. Hurst, "Long Term Storage Capacity of Reservoirs," *Trans. Amer. Soc. Civil Eng.* **116**, 770–808 (1951).
7. P. Flandrin, "On the Spectrum of Fractional Brownian Motions," *IEEE Trans. Inform. Theory* **35**, 197–199 (1989).
8. P. Flandrin, "Wavelet Analysis and Synthesis of Fractional Brownian Motion," *IEEE Trans. Inform. Theory* **38**, 910–917 (1992).
9. P. Flandrin, "Time–Scale Analyses and Self-Similar Stochastic Processes," *Proc. NATO Advanced Study Institute on Wavelets and their Applications* (Il Ciocco, Italy, 1992).

10. G. W. Wornell and A. V. Oppenheim, "Estimation of Fractal Signals from Noisy Measurements using Wavelets," *IEEE Trans. Sig. Proc.* **40**, 611–623 (1992).
11. R. J. Barton and H. V. Poor, "Signal Detection in Fractional Gaussian Noise," *IEEE Trans. Inform. Theory* **34**, 943–959 (1988).
12. W. H. Press, "Flicker Noises in Astronomy and Elsewhere," *Comm. Astrophys.* **7** (No. 4), 103–119 (1978).
13. M. J. Buckingham, *Noise in Electronic Devices and Systems* (Wiley-Halsted, New York, 1983), Ch. 6.
14. M. B. Weissman, "$1/f$ Noise and Other Slow, Nonexponential Kinetics in Condensed Matter," *Rev. Mod. Phys.* **60**, 537–571 (1988).
15. J. B. Bassingthwaighte, L. S. Liebovitch, and B. J. West, *Fractal Physiology* (American Physiological Society, New York, 1994).
16. B. J. West and W. Deering, "Fractal Physiology for Physicists: Lévy Statistics," *Phys. Rep.* **246**, 1–100 (1994).
17. C. M. Anderson and A. J. Mandell, "Fractal Time and the Foundations of Consciousness: Vertical Convergence of $1/f$ Phenomena from Ion Channels to Behavioral States," in *Fractals of Brain, Fractals of Mind* (Advances in Consciousness Research **7**), eds. E. MacCormac and M. Stamenov (John Benjamin, Amsterdam, 1996), pp. 75–128.
18. G. Pfister and H. Scher, "Dispersive (non-Gaussian) Transient Transport in Disordered Solids," *Adv. Phys.* **27**, 747–798 (1978).
19. J. Orenstein, M. A. Kastner, and V. Vaninov, "Transient Photoconductivity and Photoinduced Optical Absorption in Amorphous Semiconductors," *Phil. Mag.* **B46**, 23–62 (1982).
20. M. A. Kastner, "The Peculiar Motion of Electrons in Amorphous Semiconductors," in *Physical Properties of Amorphous Materials,* eds. D. Alser, B. B. Schwartz, and M. C. Steele (Plenum, New York, 1985), pp. 381–396.
21. T. Tiedje and A. Rose, "A Physical Interpretation of Dispersive Transport in Disordered Semiconductors," *Solid State Commun.* **37**, 49–52 (1980).
22. M. F. Shlesinger, "Fractal Time and $1/f$ Noise in Complex Systems," *Ann. New York Acad. Sci.* **504**, 214–228 (1987).
23. S. B. Lowen and M. C. Teich, "Fractal Renewal Processes Generate $1/f$ Noise," *Phys. Rev.* **E47**, 992–1001 (1993).
24. S. B. Lowen and M. C. Teich, "Fractal Renewal Processes as a Model of Charge Transport in Amorphous Semiconductors," *Phys. Rev.* **B46**, 1816–1819 (1992).
25. V. K. Bhatnagar and K. L. Bhatia, "Frequency Dependent Electrical Transport in Bismuth-Modified Amorphous Germanium Sulfide Semiconductors," *J. Non-cryst. Sol.* **119**, 214–231 (1990).
26. W. Tomaszewicz, "Multiple-Trapping Carrier Transport due to Modulated Photogeneration," *Phil. Mag. Lett.* **61**, 237–243 (1990).
27. J. M. Berger and B. B. Mandelbrot, "A New Model for the Clustering of Errors on Telephone Circuits," *IBM J. Res. Dev.* **7**, 224–236 (1963).
28. B. B. Mandelbrot, "Self-Similar Error Clusters in Communication Systems and the Concept of Conditional Stationarity," *IEEE Trans. Comm. Tech.* **13**, 71–90 (1965).
29. W. E. Leland, M. S. Taqqu, W. Willinger, and D. V. Wilson, "On the Self-Similar Nature of Ethernet Traffic," in *Proc. ACM SIGCOMM 1993* (1993), pp. 183–193.
30. A. Erramilli and W. Willinger, "Fractal Properties in Packet Traffic Measurements," in *Proc. St. Petersburg Reg. ITC Sem.* (St. Petersburg, Russia, 1993), pp. 144-158.
31. B. K. Ryu and H. E. Meadows, "Performance Analysis and Traffic Behavior of Xphone Videoconferencing Application on an Ethernet," in *Proc. 3rd Int. Conf. Comp. Commun. Netw.*, ed. W. Liu (1994), pp. 321–326.
32. W. E. Leland, M. S. Taqqu, W. Willinger, and D. V. Wilson, "On the Self-Similar Nature of Ethernet Traffic (extended version)," *IEEE/ACM Trans. Netw.* **2**, 1–15 (1994).
33. J. Beran, R. Sherman, M. S. Taqqu, and W. Willinger, "Long-Range Dependence in Variable-Bit-Rate Video Traffic," *IEEE Trans. Comm.* **43**, 1566–1579 (1995).
34. B. K. Ryu and S. B. Lowen, "Modeling Self-Similar Traffic with the Fractal-Shot-Noise-Driven Poisson Process," *Center for Telecommunications Research, Technical Report* 392-94-39 (Columbia University, New York, 1994).
35. B. Sakmann and E. Neher, *Single-Channel Recording* (Plenum, New York, 1983).
36. L. J. DeFelice and A. Isaac, "Chaotic States in a Random World: Relationship Between the Nonlinear Differential Equations of Excitability and the Stochastic Properties of Ion Channels," *J. Stat. Phys.* **70**, 339–354 (1993).
37. P. Läuger, "Internal Motions in Proteins and Gating Kinetics of Ionic Channels," *Biophys. J.* **53**, 877–884 (1988).
38. G. L. Millhauser, E. E. Salpeter, and R. E. Oswald, "Diffusion Models of Ion-Channel Gating and the Origin of Power-Law Distributions from Single-Channel Recording," *Proc. Natl. Acad. Sci.* (USA) **85**, 1503–1507 (1988).
39. L. S. Liebovitch and T. I. Tóth, "Using Fractals to Understand the Opening and Closing of Ion Channels," *Ann. Biomed. Eng.* **18**, 177–194 (1990).

40. M. C. Teich, "Fractal Character of the Auditory Neural Spike Train," *IEEE Trans. Biomed. Eng.* **36**, 150–160 (1989).
41. S. B. Lowen and M. C. Teich, "Fractal Renewal Processes," *IEEE Trans. Inform. Theory* **39**, 1669–1671 (1993).
42. S. B. Lowen and M. C. Teich, "Fractal Auditory-Nerve Firing Patterns may Derive from Fractal Switching in Sensory Hair-Cell Ion Channels," in *Noise in Physical Systems and* $1/f$ *Fluctuations* (AIP Conference Proceedings **285**), eds. P. H. Handel and A. L. Chung (American Institute of Physics, New York, 1993), pp. 781–784.
43. B. Katz, *Nerve, Muscle, and Synapse* (McGraw-Hill, New York, 1966).
44. P. Fatt and B. Katz, "Spontaneous Subthreshold Activity at Motor Nerve Endings," *J. Physiol.* (London) **117**, 109–128 (1952).
45. J. Del Castillo and B. Katz, "Quantal Components of the End-Plate Potential," *J. Physiol.* (London) **124**, 560–573 (1954).
46. S. B. Lowen, S. S. Cash, M-m. Poo, and M. C. Teich, "Neuronal Exocytosis Exhibits Fractal Behavior," in *Computational Neuroscience,* ed. J. M. Bower (Plenum, New York, 1997), pp. 13–18.
47. S. B. Lowen, S. S. Cash, M-m. Poo, and M. C. Teich, "Quantal Neurotransmitter Secretion Rate Exhibits Fractal Behavior," *J. Neurosci.* **17**, 5666–5677 (1997).
48. T. Musha, Y. Kosugi, G. Matsumoto, and M. Suzuki, "Modulation of the Time Relation of Action Potential Impulses Propagating along an Axon," *IEEE Trans. Biomed. Eng.* **BME-28**, 616–623 (1981).
49. T. Musha, H. Takeuchi, and T. Inoue, "$1/f$ Fluctuations in the Spontaneous Spike Discharge Intervals of a Giant Snail Neuron," *IEEE Trans. Biomed. Eng.* **BME-30**, 194–197 (1983).
50. S. B. Lowen and M. C. Teich, "Auditory-Nerve Action Potentials Form a Non-Renewal Point Process over Short as well as Long Time Scales," *J. Acoust. Soc. Am.* **92**, 803–806 (1992).
51. M. C. Teich, D. H. Johnson, A. R. Kumar, and R. G. Turcott, "Rate Fluctuations and Fractional Power-Law Noise Recorded from Cells in the Lower Auditory Pathway of the Cat," *Hear. Res.* **46**, 41–52 (1990).
52. M. C. Teich, R. G. Turcott, and S. B. Lowen, "The Fractal Doubly Stochastic Poisson Point Process as a Model for the Cochlear Neural Spike Train," in *The Mechanics and Biophysics of Hearing (Lecture Notes in Biomathematics, Vol. 87),* eds. P. Dallos, C. D. Geisler, J. W. Matthews, M. A. Ruggero, and C. R. Steele (Springer-Verlag, New York, 1990), pp. 354–361.
53. N. L. Powers, R. J. Salvi, and S. S. Saunders, "Discharge Rate Fluctuations in the Auditory Nerve of the Chinchilla," in *Abstracts of the Fourteenth Midwinter Research Meeting of the Association for Research in Otolaryngology,* ed. D. J. Lim (Association for Research in Otolaryngology, Des Moines, IA), Abstract 411, p. 129.
54. N. L. Powers and R. J. Salvi, "Comparison of Discharge Rate Fluctuations in the Auditory Nerve of Chickens and Chinchillas," in *Abstracts of the Fifteenth Midwinter Research Meeting of the Association for Research in Otolaryngology,* ed. D. J. Lim (Association for Research in Otolaryngology, Des Moines, IA, 1992), Abstract 292, p. 101.
55. M. C. Teich, "Fractal Neuronal Firing Patterns," in *Single Neuron Computation,* eds. T. McKenna, J. Davis, and S. Zornetzer (Academic, Boston, 1992), pp. 589–625.
56. A. H. Kumar and D. H. Johnson, "Analyzing and Modeling Fractal Intensity Point Processes," *J. Acoust. Soc. Am.* **93**, 3365–3373 (1993).
57. M. C. Teich and S. B. Lowen, "Fractal Patterns in Auditory Nerve-Spike Trains," *IEEE Eng. Med. Biol. Mag.* **13** (No. 2), 197–202 (1994).
58. O. E. Kelly, "Analysis of Long-Range Dependence in Auditory-Nerve Fiber Recordings," Master's Thesis, Rice University (1994).
59. O. E. Kelly, D. H. Johnson, B. Delgutte, and P. Cariani, "Fractal Noise Strength in Auditory-Nerve Fiber Recordings," *J. Acoust. Soc. Am.* **99**, 2210–2220 (1996).
60. S. B. Lowen and M. C. Teich, "The Periodogram and Allan Variance Reveal Fractal Exponents Greater than Unity in Auditory-Nerve Spike Trains," *J. Acoust. Soc. Am* **99**, 3585–3591 (1996).
61. S. B. Lowen and M. C. Teich, "Refractoriness-Modified Fractal Stochastic Point Processes for Modeling Sensory-System Spike Trains," in *Computational Neuroscience,* ed. J. M. Bower (Academic, New York, 1996), pp. 447-452.
62. S. B. Lowen and M. C. Teich, "Estimating Scaling Exponents in Auditory-Nerve Spike Trains using Fractal Models Incorporating Refractoriness," in *Diversity in Auditory Mechanics,* eds. E. R Lewis, G. R. Long, R. F. Lyon, P. M. Narins, C. R. Steele, and E. Hecht-Pointar (World Scientific, Singapore, 1997), pp. 197-204.
63. M. C. Teich, C. Heneghan, S. B. Lowen, T. Ozaki, and E. Kaplan, "Fractal Character of the Neural Spike Train in the Visual System of the Cat," *J. Opt. Soc. Am.* **A14**, 529–546 (1997).
64. J. B. Troy and J. G. Robson, "Steady Discharges of X and Y Retinal Ganglion Cells of Cat under Photopic Illuminance," *Visual Neuroscience* **9**, 535–553 (1992).

65. M. C. Teich, R. G. Turcott, and R. M. Siegel, "Temporal Correlation in Cat Striate-Cortex Neural Spike Trains," *IEEE Eng. Med. Biol. Mag.* **15** (No. 5), 79–87 (1996).
66. R. G. Turcott, P. D. R. Barker, and M. C. Teich, "Long-Duration Correlation in the Sequence of Action Potentials in an Insect Visual Interneuron," *J. Statist. Comput. Simul.* **52**, 253–271 (1995).
67. M. E. Wise, "Spike Interval Distributions for Neurons and Random Walks with Drift to a Fluctuating Threshold," in *Statistical Distributions in Scientific Work, Vol. 6*, eds. C. Taillie, G. P. Patil, and B. A. Baldessari (D. Reidel, Hingham, MA, 1981), pp. 211–231.
68. M. Yamamoto, H. Nakahama, K. Shima, T. Kodama, and H. Mushiake, "Markov-Dependency and Spectral Analyses on Spike-Counts in Mesencephalic Reticular Formation during Sleep and Attentive States," *Brain Research* **366**, 279–289 (1986).
69. F. Grüneis, M. Nakao, M. Yamamoto, T. Musha, and H. Nakahama, "An Interpretation of $1/f$ Fluctuations in Neuronal Spike Trains during Dream Sleep," *Biol. Cybern.* **60**, 161–169 (1989).
70. F. Grüneis, M. Nakao, Y. Mizutani, M. Yamamoto, M. Meesman, and T. Musha, "Further Study on $1/f$ Fluctuations Observed in Central Single Neurons During REM Sleep," *Biol. Cybern.* **68**, 193–198 (1993).
71. T. Kodama, H. Mushiake, K. Shima, H. Nakahama, and M. Yamamoto, "Slow Fluctuations of Single Unit Activities of Hippocampal and Thalamic Neurons in Cats. I. Relation to Natural Sleep and Alert States," *Brain Research* **487**, 26–34 (1989).
72. M. Yamamoto and H. Nakahama, "Stochastic Properties of Spontaneous Unit Discharges in Somatosensory Cortex and Mesencephalic Reticular Formation during Sleep–Waking States," *J. Neurophysiology* **49**, 1182–1198 (1983).
73. M. Kobayashi and T. Musha, "$1/f$ Fluctuations of Heartbeat Period," *IEEE Trans. Biomed. Eng.* **BME-29**, 456–457 (1982).
74. R. D. Berger, S. Akselrod, D. Gordon, and R. J. Cohen, "An Efficient Algorithm for Spectral Analysis of Heart Rate Variability," *IEEE Trans. Biomed. Eng.* **BME-33**, 900–904 (1986).
75. R. G. Turcott and M. C. Teich, "Long-Duration Correlation and Attractor Topology of the Heartbeat Rate Differ for Healthy Patients and Those with Heart Failure," *Proc. SPIE* **2036** (Chaos in Biology and Medicine), 22–39 (1993).
76. R. G. Turcott and M. C. Teich, "Interevent-Interval and Counting Statistics of the Human Heartbeat Recorded from Normal Subjects and Patients with Heart Failure," *Ann. Biomed. Eng.* **24**, 269–293 (1996).
77. H. E. Schepers, J. H. G. M. van Beek, and J. B. Bassingthwaighte, "Four Methods to Estimate the Fractal Dimension from Self-Affine Signals," *IEEE Eng. Med. Biol. Mag.* **11**, 57–64 (1992).
78. J. Beran, "Statistical Methods for Data with Long-Range Dependence," *Statistical Science* **7**, 404–427 (1992).
79. H. G. E. Hentschel and I. Procaccia, "The Infinite Number of Generalized Dimensions of Fractals and Strange Attractors," *Physica* **D8**, 435–444 (1983).
80. P. Grassberger, "Generalized Dimensions of Strange Attractors," *Phys. Lett.* **A97**, 227-230 (1983).
81. J. Theiler, "Estimating Fractal Dimension," *J. Opt. Soc. Am.* **A7**, 1055–1073 (1990).
82. K. Matsuo, B. E. A. Saleh, and M. C. Teich, "Cascaded Poisson Processes," *J. Math. Phys.* **23**, 2353–2364 (1982).
83. S. B. Lowen and M. C. Teich, "Estimating the Dimension of a Fractal Point Processes," *Proc. SPIE* **2036** (Chaos in Biology and Medicine), 64–76 (1993).
84. D. W. Allan, "Statistics of Atomic Frequency Standards," *Proc. IEEE* **54**, 221-230 (1966).
85. J. A. Barnes and D. W. Allan, "A Statistical Model of Flicker Noise," *Proc. IEEE* **54**, 176–178 (1966).
86. M. C. Teich, C. Heneghan, S. B. Lowen, and R. G. Turcott, "Estimating the Fractal Exponent of Point Processes in Biological Systems using Wavelet- and Fourier-Transform Methods," in *Wavelets in Medicine and Biology*, eds. A. Aldroubi and M. Unser (CRC Press, Boca Raton, FL, 1996), pp. 383–412.
87. C. Heneghan, S. B. Lowen, and M. C. Teich, "Wavelet Analysis for Estimating the Fractal Properties of Neural Firing Patterns," in *Computational Neuroscience*, ed. J. M. Bower (Academic Press, San Diego, 1996), pp. 441–446.
88. S. B. Lowen, "Refractoriness-Modified Doubly Stochastic Poisson Point Process," *Center for Telecommunications Research, Technical Report* **449-96-15** (Columbia University, New York, 1996).
89. S. B. Lowen and M. C. Teich, "Doubly Stochastic Poisson Point Process Driven by Fractal Shot Noise," *Phys. Rev.* **A43**, 4192–4215 (1991).
90. F. Grüneis and H.-J. Baiter, "More Detailed Explication of a Number Fluctuation Model Generating $1/f$ Pattern," *Physica* **136A**, 432–452 (1986).
91. F. A. Haight, *Handbook of the Poisson Distribution* (Wiley, New York, 1967).
92. B. B. Mandelbrot, "A Fast Fractional Gaussian Noise Generator," *Water Resources Res.* **7**, 543–553 (1971).
93. T. Lundahl, W. J. Ohley, S. M. Kay, and R. Siffert, "Fractional Brownian Motion: A Maximum

Likelihood Estimator and its Application to Image Texture," *IEEE Trans. Med. Imag.* **5**, 152–161 (1986).
94. M. A. Stoksik, R. G. Lane, and D. T. Nguyen, "Accurate Synthesis of Fractional Brownian Motion using Wavelets," *Electron. Lett.* **30**, 383–384 (1994).
95. B. E. A. Saleh, *Photoelectron Statistics* (Springer Verlag, Berlin, 1978).
96. S. B. Lowen and M. C. Teich, "Generalised $1/f$ Shot Noise," *Electron. Lett.* **25**, 1072–1074 (1989).
97. S. B. Lowen and M. C. Teich, "Fractal Shot Noise," *Phys. Rev. Lett.* **63**, 1755–1759 (1989).
98. S. B. Lowen and M. C. Teich, "Power-Law Shot Noise," *IEEE Trans. Inform. Theory* **36**, 1302–1318 (1990).
99. D. R. Cox, "Some Statistical Methods Connected with Series of Events," *J. Roy. Stat. Soc.* **B17**, 129–164 (1955).
100. F. Grüneis, "A Number Fluctuation Model Generating $1/f$ Pattern," *Physica* **123A**, 149–160 (1984).
101. F. Grüneis and T. Musha, "Clustering Poisson Process and $1/f$ Noise," *Jpn. J. Appl. Phys.* **25**, 1504–1509 (1986).
102. J. Skilling, ed., *Maximum Entropy and Bayesian Methods* (Kluwer, Boston, 1988).

## APPENDIX: PSD FOR THE FGNIF PROCESS

Equation (32) yields predictions for the PG-based fractal exponent estimation bias for a general fractal-rate stochastic point process (FRSPP). More accurate results may be obtained for particular FRSPPs, taking into account the structure of these individual processes. We consider the case of the FGNIF process, with the further specialization that the original FGN array is obtained by direct Fourier synthesis with half of the array discarded, and that the analyzing periodogram subsequently doubles the number of points, yielding the same number as in the original array.

We begin with a discrete-time power spectral density $S_X(n)$ which is periodic with period $M$, and with $S_X(0) = 0$. For simulation purposes we define a conjugate symmetric sequence $\tilde{X}_n$ based on the square root of $S_X(n)$:

$$\tilde{X}_n = \begin{cases} 0 & \text{for } n = 0 \\ \exp(j\theta_n)\sqrt{S_X(n)} & \text{for } 0 < n < M/2 \\ \operatorname{sgn}(\theta_n - \pi)\sqrt{S_X(n)} & \text{for } n = M/2 \\ \tilde{X}^*_{M-n} & \text{for } M/2 < n < M, \end{cases} \tag{35}$$

where $\{\theta_n\}$ are independent and uniformly distributed in $[0, 2\pi)$, $\operatorname{sgn}(\cdot)$ represents the signum function, and $^*$ denotes complex conjugation. The corresponding time-domain signal may be obtained by inverse Fourier transformation:

$$X_k \equiv M^{-1} \sum_{n=0}^{M-1} e^{j2\pi nk/M} \tilde{X}_n \,. \tag{36}$$

We next define a subsampled sequence $Z_k$, also of length $M$, by

$$Z_k = \begin{cases} X_{k/2} & \text{for } k \text{ even} \\ X_{(k-1)/2} & \text{for } k \text{ odd}, \end{cases} \tag{37}$$

for which the corresponding sequence in the frequency domain becomes

$$\begin{aligned} \tilde{Z}_n &\equiv \sum_{k=0}^{M-1} Z_k e^{-j2\pi kn/M} \\ &= \sum_{l=0}^{M/2-1} X_l \left[ e^{-j2\pi(2l)n/M} + e^{-j2\pi(2l+1)n/M} \right] \\ &= 2e^{-j\pi n/M} \cos(\pi n/M) \sum_{l=0}^{M/2-1} X_l e^{-j4\pi ln/M} \\ &= 2M^{-1} e^{-j\pi n/M} \cos(\pi n/M) \sum_{l=0}^{M/2-1} e^{-j4\pi ln/M} \sum_{q=1}^{M-1} e^{j2\pi ql/M} \tilde{X}_q \,. \end{aligned} \tag{38}$$

Finally, we compute the expected value of the periodogram of $Z$

$$\begin{aligned}
\mathrm{E}\left[\widehat{S_Z}(n)\right] &\equiv M^{-1}\mathrm{E}\left[\tilde{Z}_n\right]^2 \\
&= 4M^{-3}\cos^2(\pi n/M)\sum_{l=0}^{M/2-1} e^{-j4\pi ln/M}\sum_{k=0}^{M/2-1} e^{j4\pi kn/M} \\
&\quad\times\sum_{q=1}^{M-1} e^{j2\pi ql/M}\sum_{r=1}^{M-1} e^{-j2\pi rk/M}\mathrm{E}\left[\tilde{X}_q\tilde{X}_r^*\right] \\
&= 4M^{-2}\cos^2(\pi n/M)\sum_{l=0}^{M/2-1} e^{-j4\pi ln/M}\sum_{k=0}^{M/2-1} e^{j4\pi kn/M}\sum_{q=1}^{M-1} e^{j2\pi ql/M}e^{-j2\pi qk/M}S_X(q) \\
&= 4M^{-2}\cos^2(\pi n/M)\sum_{q=1}^{M-1} S_X(q)\left|\sum_{l=0}^{M/2-1} e^{-j2\pi(2n-q)l/M}\right|^2 \\
&= \cos^2(\pi n/M)\left\{S_X(2n) + 4M^{-2}\sum_{\substack{q=1\\ q\ \text{odd}}}^{M-1}\csc^2\left[\pi(2n-q)/M\right]S_X(q)\right\}. \qquad (39)
\end{aligned}$$

Numerical computation based on Eq. (39) yields results substantially in agreement with those of Eq. (32).